Published December 13, 2018

Special Section: Hydrological Observatories

Core Ideas

- Heihe was the first basin-scale integrated observatory network established in China.
- An intensive flux observation matrix experiment was conducted.
- New techniques, e.g., wireless sensor network, flux matrix, and airborne remote sensing, are used.
- The integrated observatory network is useful in land surface processes research.

S. Liu, Z. Xu, T. Xu, and Z. Zhu, State Key Lab. of Earth Surface Processes and Resource Ecology, Faculty of Geographical Science, Beijing Normal Univ., Beijing 100875, China; X. Li, T. Che, R. Jin, J. Guo, W. Wang, Y. Qi, H. Li, Y. Ran, X. Hu, J. Tan, Y. Zhang, and Z. Ren, Cold and Arid Regions Environmental and Engineering Research Institute, Chinese Academy of Sciences, Lanzhou 730000, China; Q. Xiao and Q. Liu, State Key Lab. of Remote Sensing Science, Institute of Remote Sensing and Digital Earth, Chinese Academy of Sciences, Beijing 100101, China; M. Ma, Research Base of Karst Eco-environments at Nanchuan in Chongqing, Ministry of Nature Resources, School of Geographical Sciences, Southwest Univ., Beibei, Chongqing 400715, China; L. Wang, Institute of Urban Studies, Shanghai Normal Univ., Shanghai 200234, China; S. Shi, College of Resources and Environmental Sciences, China Agricultural Univ., Beijing 100193, China. *Corresponding author (smliu@bnu.edu.cn).

Received 6 Apr. 2018.
Accepted 1 Nov. 2018.

Citation: Liu, S., X. Li, Z. Xu, T. Che, Q. Xiao, M. Ma, Q. Liu, R. Jin, J. Guo, L. Wang, W. Wang, Y. Qi, H. Li, T. Xu, Y. Ran, X. Hu, S. Shi, Z. Zhu, J. Tan, Y. Zhang, and Z. Ren. 2018. The Heihe Integrated Observatory Network: A basin-scale land surface processes observatory in China. Vadose Zone J. 17:180072. doi:10.2136/vzj2018.04.0072

The Heihe Integrated Observatory Network: A Basin-Scale Land Surface Processes Observatory in China

Shaomin Liu,* Xin Li, Ziwei Xu, Tao Che, Qing Xiao, Mingguo Ma, Qinhuo Liu, Rui Jin, Jianwen Guo, Liangxu Wang, Weizhen Wang, Yuan Qi, Hongyi Li, Tongren Xu, Youhua Ran, Xiaoli Hu, Shengjin Shi, Zhongli Zhu, Junlei Tan, Yang Zhang, and Zhiguo Ren

Research on land surface processes at the catchment scale has drawn much attention over the past few decades, and a number of watershed observatories have been established worldwide. The Heihe River Basin (HRB), which contains the second largest inland river in China, is an ideal natural field experimental area for investigation of land surface processes involving diverse landscapes and the coexistence of cold and arid regions. The Heihe Integrated Observatory Network was established in 2007. For long-term observations, a hydrometeorological observatory, ecohydrological wireless sensor network, and satellite remote sensing are now in operation. In 2012, a multiscale observation experiment on evapotranspiration over heterogeneous land surfaces was conducted in the midstream region of the HRB, which included a flux observation matrix, wireless sensor network, airborne remote sensing, and synchronized ground measurements. Under an open data policy, the datasets have been publicly released following careful data processing and quality control. The outcomes highlight the integrated research on land surface processes in the HRB and include observed trends, scaling methods, high spatiotemporal resolution remote sensing products, and model–data integration in the HRB, all of which are helpful to other endorheic basins in the "Silk Road Economic Belt." Henceforth, the goal of the Heihe Integrated Observatory Network is to develop an intelligent monitoring system that incorporates ground-based observatory networks, unmanned aerial vehicles, and multi-source satellites through the Internet of Things technology. Furthermore, biogeochemical processes observation will be improved, and the study of integrating ground observations, remote sensing, and large-scale models will be promoted further.

Abbreviations: ASTER, Advanced Spaceborne Thermal Emission and Reflection Radiometer; EC, eddy covariance; ET, evapotranspiration; FIFE, First International Satellite Land Surface Climatology Project Field Experiment; FVC, fractional vegetation cover; HiWATER, Heihe Watershed Allied Telemetry Experimental Research; HiWATER-MUSOEXE, Heihe Watershed Allied Telemetry Experimental Research–Multi-Scale Observation Experiment on Evapotranspiration over Heterogeneous Land Surfaces Experiment; HRB, Heihe River Basin; LAI, leaf area index; LAS, large aperture scintillometer; LST, land surface temperature; MODIS, Moderate Resolution Imaging Spectroradiometer; PAR, photosynthetically active radiation; TSEB, two-source energy balance model; WATER, Watershed Allied Telemetry Experimental Research; WSN, wireless sensor network.

Understanding the interactions among water, soil, atmosphere, biology, and human behavior in land surface processes is highly significant. To improve our knowledge and understanding of land surface processes, it is necessary to conduct field observation experiments in various climatic zones. Under the coordinated organization of the World Climate Research Program and the International Geosphere–Biosphere Program, several large experiments to investigate land surface processes have been conducted worldwide since the 1980s. These studies have been recognized as milestones that have advanced our understanding of the Earth surface system, including the First International Satellite Land Surface Climatology Project Field Experiment (FIFE, United States; Sellers et al., 1988), the Hydrologic Atmospheric

Pilot Experiment (HAPEX, France; André et al., 1986); HAPEX-Sahel (Niger; Goutorbe et al., 1994), the Northern Hemisphere Climate Processes Land Surface Experiment (NOPEX, Sweden; Halldin et al., 1999), and the Boreal Ecosystem–Atmosphere Study (BORAS, Canada; Sellers et al., 1995). Similar experiments have been conducted in China since the late 1980s, including the Heihe River Basin Field Experiment (HEIFE; Hu et al., 1994; Wang, 1999), the Inner Mongolia Semiarid Grassland Soil–Vegetation–Atmosphere Interaction (IMGRASS; Lv et al., 2002), the Global Energy and Water Cycle Experiment Asian Monsoon Experiment on the Tibetan Plateau (GAME/Tibet, Ma et al., 2006), and the Huaihe River Basin Energy and Water Cycle Experiment (GAME/HUBEX, Zhang, 1998). Most of these field experiments focused on interactions between land surfaces and the atmosphere and were typically conducted in a specific area during relatively short time periods. The primary objective of these studies was to assist the parameterization of sub-grid processes for general circulation or land surface models via detailed local observations.

In the mid-1990s, the global network FLUXNET was established (Baldocchi et al., 1996), which includes the areas of North and South America, Europe, Asia, Oceania, and Africa and covers land surfaces including forest, cropland, grassland, jungle, wetland, and tundra, etc. By February 2017, there were 914 registered sites (covering 7479 site years). FLUXNET observations are mainly intended to monitor the carbon cycle, water vapor, and energy exchanges between the surface and atmosphere and to provide basic validation data for remote sensing products (e.g., evapotranspiration [ET] and net primary productivity). FLUXNET achieves a transition from single site to multiple sites, allowing the formation of a long-term observation network. However, FLUXNET has not been well integrated into a close alliance because the management and operation of each site is relatively independent.

During the past decade, distributed observation systems at the watershed scale have become increasingly popular (Cheng et al., 2014a; Cheng and Li, 2015); the catchment scale is currently considered to be the most appropriate scale for water legislation and management (Jensen and Illangasekare, 2011). A number of environmental observatories at the catchment scale have been established across the world, and these represent various climatic, hydrologic, topographic, and land cover conditions. In Germany, a Terrestrial Environmental Observatories (TERENO) network initiative was implemented in 2008 (Zacharias et al., 2011; Bogena et al., 2015). In 2007, the Danish hydrological observatory (HOBE) was established (Jensen and Illangasekare, 2011), and the Critical Zone Observatories network, including nine observatories, was launched in the United States (Lin et al., 2011). In addition, basins have been used as the unit to construct national observation platforms, including the National Ecological Observatory Network (NEON) in the United States (Kuhlman et al., 2016) and the Terrestrial Ecosystem Research Network (TERN) in Australia (Phinn et al., 2011). The characteristics of these distributed observation systems are defined by the nature of many variables, multiscales, and satellite–airborne–ground observations. The observation platforms involve optimization designs closely connected to the associated information systems and integrated into a long-term, distributed monitoring system across sites. Such distributed observation systems can provide insightful information for model development and observation data analysis, while remote sensing (especially airborne remote sensing) acts as a bridge for scaling.

The HRB is the second largest endorheic basin in the arid region of northwestern China. Air temperature and precipitation show obvious zonal characteristics as the elevation changes from upstream to downstream regions. Cold and arid regions coexist in the basin, forming a sharp contrast between the mountainous cryosphere and extreme drought in the terminal lake region. Moreover, the water cycle can be closed in the inland rivers, and the hydrological environment has been significantly influenced by human activities, such as farm development, wasteland reclamation, dam operations, and the convergence of natural and cultural processes. These characteristics make the HRB an ideal natural field experimental area to further pursue integrated observation and research on land surface processes and will benefit the natural ecosystem and society and expand scientific research on watersheds and remote sensing research for cold and arid regions (Li et al., 2013). In addition, the HRB is the largest river basin in the National Nature Reserve of the Qilian Mountains and is located in the core area of the "Silk Road Economic Belt." Along the Silk Road to the west, several endorheic basins exist, such as the Tarim River basin and the Amu Darya River basin in central Asia. These endorheic basins have similar geographical environments and face the same water resource issues. Therefore, the observations and research findings from the HRB will serve as references and representatives for other endorheic basins in the area of "The Belt and Road Initiative" and "The Pan-Third Pole" (Yao et al., 2017a).

A major research plan entitled "Integrated research on the eco-hydrological process of the Heihe River Basin" was launched by the National Natural Science Foundation of China in 2010. One of the key goals of this research plan was to establish a research platform that integrates observations, data management, and model simulation, representing the frontiers in watershed science in China (Li et al., 2013). Several comprehensive experiments such as the Heihe basin fields experiment (Hu et al., 1994), the Jinta experiment (Ao et al., 2005), the Watershed Allied Telemetry Experimental Research (WATER, Li et al., 2009), and the Heihe Watershed Allied Telemetry Experimental Research (HiWATER, Li et al., 2013) have been conducted in the HRB. Here we review the history of long-term observations in the HRB since 2007 and the dedicated campaigns and experiments that were conducted mainly in 2012. Additionally, data processing and management policies are also introduced. Finally, new insight and scientific findings are summarized, and future perspectives are outlined.

Scientific Questions and Motivation

The HRB is a complex system having unique biological and environmental characteristics and encompasses diverse landscapes

including ice–frozen soil–snow, forests, grasslands, oases, deserts, and lakes. Water plays an important role by connecting the entire basin. Specific scientific questions concerning the HRB include (Cheng et al., 2014b): (i) water use efficiency of plants under drought conditions and its adaptation mechanism to water stress; (ii) groundwater–surface water interaction and their eco-hydrological effects; (iii) eco-hydrological processes across scales and the scaling issues; (iv) the responses of watershed eco-hydrological processes under climate change and human activities; and (v) integrating comprehensive observational data and modeling. Under the frameworks of the WATER and HiWATER experiments, the goals of the Heihe integrated observatory network include (i) building a world-class multi-element, multiscale, networked, and elaborated integrated observatory to improve the observability of land surface processes in the basin; (ii) constructing a remote sensing validation site for typical land surfaces in cold and arid regions to form a multiscale observation platform (point–footprint–remote sensing pixel–catchment scale); and (iii) conducting integrated observations encompassing ground measurements and remote sensing data to accumulate a long-term observation dataset. This will aid the integrated research on land surface processes in cold and arid regions and enhance the applicability of remote sensing for integrated research on land surface processes and water resource management at the basin scale.

Catchment Characteristics of the Heihe River Basin

The HRB is an endorheic basin located in the arid and semiarid regions of Northwest China (Fig. 1a) that covers three Chinese provinces: Qinghai Province (upstream), Gansu Province (midstream), and Inner Mongolia Autonomous Region (downstream). The HRB is located at 97.1 to 102.0° E and 37.7 to 42.7° N and covers an area of approximately 143,000 km^2. The HRB rises near the central Qilian Mountains. It is bounded by the Sino-Mongolian border to the north, the Shiyang River basin to the east, the Shule River basin to the west, and is adjacent to the Datong-Huangshui and the Qinghai Lake basin to the south.

The elevation of the HRB decreases from south to north, ranging from approximately 2000 to 5000 m in the upstream region to 1000 to 3000 m in the midstream region, and 800 to 1700 m in the downstream region (Fig. 1a). The land use and cover types in the HRB are diverse. The main land uses or covers in the upstream region are glaciers (0.5% of the HRB), grasslands (alpine meadow, 10.1%), and evergreen needle-leaved forests (including Qinghai spruce [*Picea crassifolia*], 0.5%); in the midstream region, the land covers include croplands (including maize [*Zea mays* L.], 3.6%) and barren lands (piedmont desert, 29.4%); in the downstream region, the land cover consists of mixed forests and shrubs (including *Populus euphratica* Oliv. and *Tamarix*, 0.2%), barren lands (desert, 55.1%), and water bodies (terminal lake, 0.3%); other land uses or covers include cities, towns, and residential areas (0.3%) (Fig. 1b).

Miscellaneous soil types are spatially distributed in the HRB. In the upstream region, the main soil types include Gelic Cambosols, Ustic Isohumosols, and Orthic Aridosols, while in the midstream and downstream regions, soil types include Sandic Primosols and Calci-orthic Aridosols (Cheng, 2009). Regarding soil particle composition, the upstream region clay content is 11.2% at the surface soil layer (0–5 cm), and the sand content is 27.9%. Midstream region soils are similar, with clay content of 10.0% and sand content of 39.9%. Sand content is dominant in the downstream region, averaging of 63.4%—distinctly higher than in the upstream and midstream regions (Fig. 1c and 1d) (Yang et al., 2016; Song et al., 2016).

The Heihe River originates in the Qilian Mountains, extending approximately 928 km from upstream to downstream. The upstream region is a runoff area, while the midstream and downstream regions are water consumption areas. The average annual streamflow measured at the Yingluo Gorge (an upstream outlet) was 15.97 × 10^8 m^3 yr^{-1} from 1945 to 2012. The limited water resources in this region are mainly used to irrigate the oases, specifically for cropland irrigation in the artificial oasis in the midstream region and for ecological water demand in the natural oasis in the downstream region. The climate of the HRB is dry, with scarce precipitation, ample sunshine, and strong winds. There are clear differences in the climatic characteristics among the upstream, midstream, and downstream regions. In the upstream region, the annual mean temperature, relative humidity, and wind speed are 2.3°C, 53.2%, and 1.9 m s^{-1}, respectively, and the annual precipitation exceeds 500 mm (Qilian County, 1960–2015). In addition, seasonal snow cover dominates in the upstream region. During 2001 to 2012, the snow cover almost disappeared in summer, except for areas of transient snow and glaciers covering 236 to 830 km^2. Monthly snow cover had a maximum of 3567 km^2 in March. The interannual variation in snowmelt was 15%, which played an important role in sustaining the total streamflow (Li et al., 2018b). In the midstream region, the annual mean temperature, relative humidity, and wind speed are 8.2°C, 51.4%, and 2.1 m s^{-1}, respectively, and the annual precipitation exceeds 150 mm (Zhangye wetland, 1960–2015). In the downstream region, the annual mean temperature, relative humidity, and wind speed are 9.4°C, 33.7%, and 3.2 m s^{-1}, respectively, and the annual precipitation is approximately 50 mm (Ejin Banner oasis, 1960–2015).

Long-Term Observations

The Heihe integrated observatory network was first established in 2007 during the WATER experiment (2007–2011; Li et al., 2009) and was completed in 2013 during the HiWATER experiment (2012–2015; Li et al., 2013) under the framework of the "Integrated research on the eco-hydrological process of the Heihe River Basin" project supported by the National Natural Science Foundation of China. Since 2016, it has been refined into a mature shape and has entered into a regular operational phase. The observatory includes long-term observations and dedicated campaigns and experiments. The long-term observations of the Heihe Integrated Observatory Network comprise the

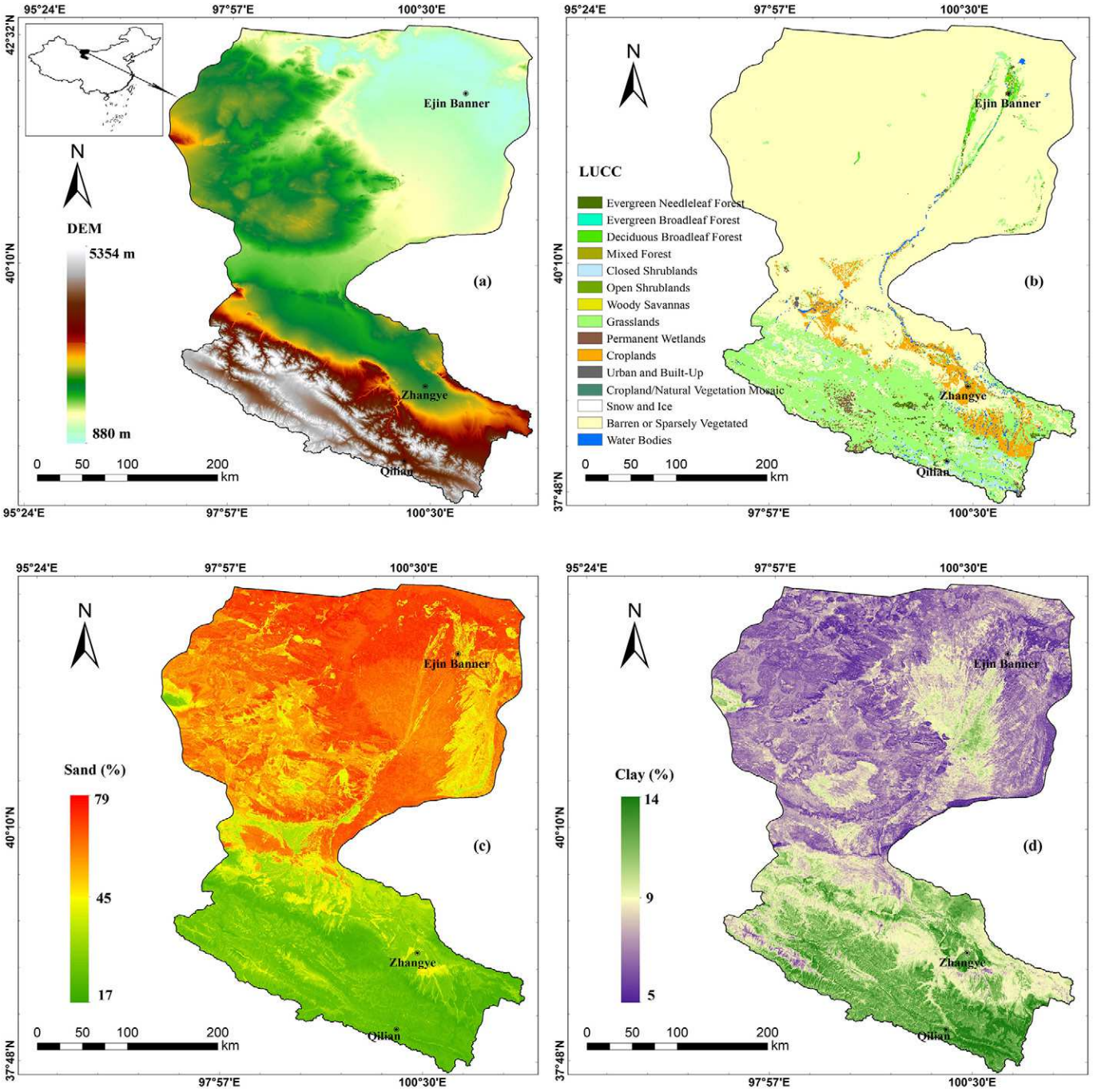

Fig. 1. (a) Digital elevation model (DEM), (b) land use and cover classification (LUCC), and proportions of (c) sand and (d) clay in the soil of the Heihe River Basin.

hydrometeorological observatory, the eco-hydrological wireless sensor network, and satellite remote sensing.

The Hydrometeorological Observatory

The hydrometeorological observatory includes at most 23 observation stations (three superstations and 20 ordinary stations) covering the main land surfaces in the HRB (Liu et al., 2011; Li et al., 2013; Liu and Xu, 2018), including alpine meadows, forestlands, croplands, deserts, bare lands, and wetlands (Table 1; Fig. 2). In 2016, the number of stations was reduced to 11 carrying out refined observations, including four stations in the upstream region (no. 1, 5, 7, and 9 in Table 1), four in the midstream region (no. 11, 13, 14, and 15 in Table 1), and three in the downstream region (no. 18, 20, 23 in Table 1).

Surface Fluxes and Meteorological Elements

The surface fluxes and meteorological elements were derived from superstations and ordinary stations that encompass the entire HRB.

Table 1. Hydrometeorological observatory stations (Arou, Daman, and Sidaoqiao are superstations; the other stations are ordinary stations).

No.	Station	Landscape	Location	Longitude	Latitude	Elevation	Duration
				——————° ——————		m	
1	Jingyangling	alpine meadow	upstream	101.12	37.84	3750	Aug. 2013–present
2	E'bao	alpine meadow	upstream	100.92	37.95	3294	June 2013–Oct. 2016
3	Huangcaogou	alpine meadow	upstream	100.73	38.00	3137	June 2013–Apr. 2015
4	Arou Sunny Slope	alpine meadow	upstream	100.52	38.09	3529	Aug. 2013–Aug. 2015
5	Arou	subalpine meadow	upstream	100.46	38.05	3033	June 2008–present
6	Arou Shady Slope	alpine meadow	upstream	100.41	37.98	3536	Aug. 2013–Aug. 2015
7	Yakou	alpine meadow	upstream	100.24	38.01	4148	Jan. 2014–present
8	Huangzangsi	wheat	upstream	100.19	38.23	2612	June 2013–Apr. 2015
9	Dashalong	marsh alpine meadow	upstream	98.94	38.84	3739	Aug. 2013–present
10	Guantan	Qinghai spruce	upstream	100.25	38.53	2835	2008–2011
11	Huazhaizi Desert Steppe	*Kalidium foliatum* desert	midstream	100.32	38.77	1731	June 2012–present
12	Shenshawo Sandy Desert	sandy desert	midstream	100.49	38.79	1594	June 2012–Apr. 2015
13	Heihe Remote Sensing	grassland	midstream	100.48	38.83	1560	Aug. 2014–present
14	Zhangye wetland	reed	midstream	100.45	38.98	1460	June 2012–present
15	Daman	maize	midstream	100.37	38.86	1556	May 2012–present
16	Yingke	maize	midstream	100.41	38.86	1519	2008–2011
17	Bajitan Gobi	*Reaumuria* desert	midstream	100.30	38.92	1562	May 2012–Apr. 2015
18	Mixed Forest	*Populus euphratica* and *Tamarix*	downstream	101.13	41.99	874	July 2013–present
19	Barren Land	bare land	downstream	101.13	42.00	878	July 2013–Mar. 2016
20	Sidaoqiao	Tamarix	downstream	101.14	42.00	873	July 2013–present
21	Cropland	melon	downstream	101.13	42.00	875	July 2013–Nov. 2015
22	Populus euphratica	*Populus euphratica*	downstream	101.12	41.99	876	July 2013–Apr. 2016
23	Desert	*Reaumuria* desert	downstream	100.99	42.11	1054	Apr. 2015–present

The superstations include a multiscale observation system for surface fluxes (sensible heat, latent heat, and CO_2 fluxes) and soil moisture measurements, which is comprised of a lysimeter (meter scale)–eddy covariance (EC) system (with a scale of hundreds of meters)–large aperture scintillometer (LAS, at kilometer scale), an in situ soil moisture sensor (meter scale)–cosmic-ray probe (with scale of hundreds of meters)–soil moisture and temperature wireless sensor network (WSN1, at kilometer scale) (Fig. 3a). It also includes a meteorological gradient observation system (six or seven layers of wind speed and direction and air temperature and humidity, precipitation, air pressure, infrared temperature, four-component radiation, photosynthetically active radiation (PAR), soil heat flux, soil temperature–moisture profile, average soil temperature, etc.). The path length of the LAS is more than one and a half times that of Moderate Resolution Imaging Spectroradiometer (MODIS) pixels (i.e., >1.5 km). The source area of the LAS is perpendicular to the prevailing wind direction, and its representative area is similar to that of MODIS pixels. The flux towers generally have heights of 30 to 40 m. As an example, the Daman superstation (40-m tower) has one lysimeter, one EC system (4.5 m), one group of LAS (two sets, effective height: 22.5 m; path length: 1854 m), one cosmic-ray probe, and nine soil temperature–moisture WSN nodes. The 40-m flux tower includes seven layers of wind speed and direction, air temperature and humidity, and CO_2 and water vapor concentration (3, 5, 10, 15, 20, 30, and 40 m) sensors, precipitation instrumentation (1.8 m; above the canopy), an air pressure instrument, two infrared temperature sensors (12 m), one four-component radiometer (12 m), four PAR sensors (0.5 m [two sets] in the canopy and 12 m [two sets] over the canopy), three soil heat flux plates under the flux tower (0.06 m; two plates buried under bare soil between maize plants and one plate buried under the maize plants), nine soil temperature and eight soil moisture sensors (0.02, 0.04, 0.1, 0.2, 0.4, 0.8, 1.2, and 1.6 m, with one soil temperature measurement sensor at the surface), and an average soil temperature sensor (0.02 and 0.04 m) (Fig. 3b).

The ordinary stations comprise an EC system and an automatic weather station that monitors surface fluxes (sensible heat, latent heat, and CO_2 fluxes; CH_4 flux is also observed in the Zhangye wetland station), wind speed and direction, air temperature and humidity, precipitation, air pressure, infrared temperature, four-component radiation, PAR, soil heat flux, soil temperature–moisture profile, etc. The heights of the flux towers are generally 10 m. As an example, the Huazhaizi desert steppe station includes one EC system (4.5 m), two-layered wind speed and direction and air temperature and humidity sensors (5 and 10 m), a two-layered rain gauge (2 and 10 m), one air pressure instrument, two infrared

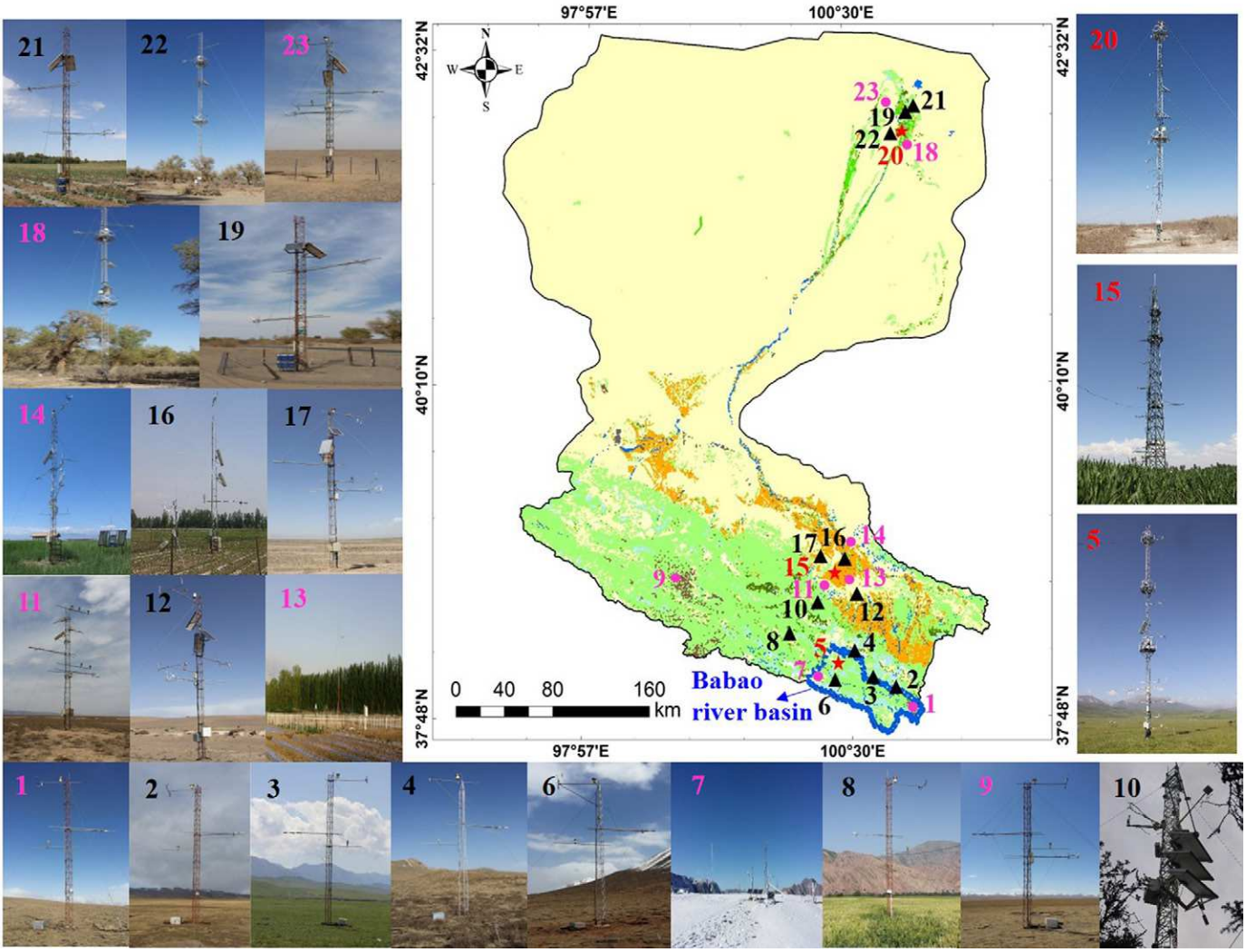

Fig. 2. The hydrometeorological observatory in the Heihe River Basin (red stars: superstations; pink circles: operating ordinary stations; black triangles: removed ordinary stations). The station numbers correspond to those in Table 1.

temperature sensors (6 m), one four-component radiometer (6 m), three soil heat flux plates (0.06 m), and eight soil temperature and seven soil moisture sensors (0.02, 0.04, 0.1, 0.2, 0.4, 0.6, 1.0 m, with one soil temperature sensor at the surface) (Fig. 3c).

Snow and Frozen Soil

To accurately capture the process of snow accumulation and ablation, a snow observatory has been constructed at the Yakou station (Fig. 4) in the upstream region. In July 2013, a γ-ray monitor, which measures the snow water equivalent with a footprint of 100 m^2; a snow properties analysis system (Snow Pack Analyzer), which monitors the snow density profile and water content; a weighing precipitation and snow gauge; a set of EC systems that measures ET and sublimation on the snow surface; two snow drift monitors; and a FlowCapt sensor that measures the blowing snow flux and frictional velocity of snow drift particles were installed. An international standard precipitation gauge (with double fence intercomparison reference, DFIR) was installed in 2016 to measure precipitation and snow, and the Global Navigation Satellite System snow observation system, which measures snow depth via GPS signals, was also installed during the same period. Meanwhile, weighing precipitation and snow gauges were installed at the Arou, Jingyangling, and Dashalong stations in the upstream region, a DFIR system was also installed at the Arou superstation, and a DFIR system will be installed at the Dashalong station in 2018.

A frozen soil observatory is located at the Arou superstation. Soil temperature and moisture profiles (0.02, 0.04, 0.06, 0.1, 0.15, 0.2, 0.3, 0.4, 0.6, 0.8, 1.2, 1.6, 2.0, 2.4, 2.8, and 3.2 m, with one soil temperature sensor at 0 m) and water potential and thermal conductivity sensors (0.04, 0.1, 0.2, 0.4, 0.8, and 1.2 m) are used to monitor the freeze–thaw process. In addition, a cosmic-ray probe is used to measure soil moisture and snow water equivalent at the footprint scale of approximately 700-m diameter. The depths of the soil temperature and moisture profiles reach 1.6 m at other stations in the upstream region.

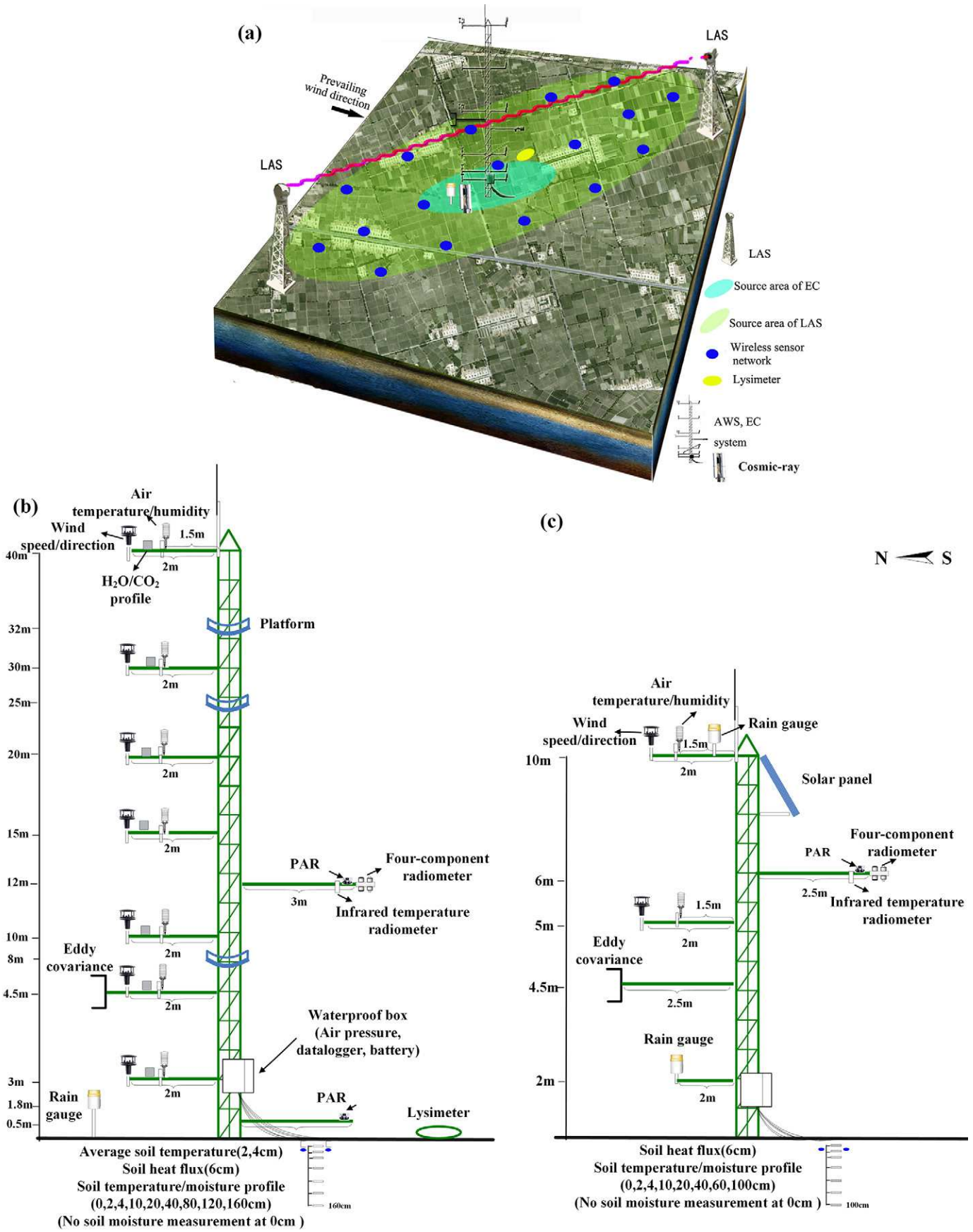

Fig. 3. Layout of (a,b) a superstation and (c) an ordinary station (LAS, large aperture scintillometer; EC, eddy covariance; AWS, automatic weather station; PAR, photosynthetically active radiation).

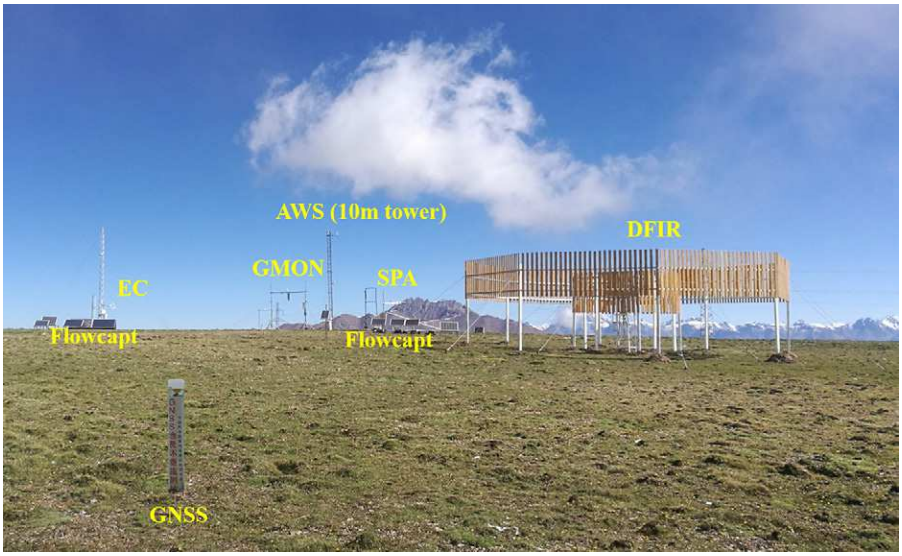

Fig. 4. The snow observatory at Yakou station, showing the automatic weather station (AWS), the eddy covariance tower (EC), two FlowCapt snowdrift and solid particle flux sensors, the global navigation satellite system (GNSS), gamma monitor (GMON), snowpack analyzer (SPA), and double fence intercomparison reference (DFIR).

Plant Eco-physiological Parameters

Three groups of thermal dissipation probes for measuring sap flow have been installed in the downstream region near the Sidaoqiao, mixed forest, and *Populus euphratica* stations to monitor the transpiration of *Populus euphratica* according to different heights and diameters at breast height since August 2013.

The parameters of phenology (2013–2017, entire basin), fractional vegetation cover (FVC, 2013–2014, midstream), plant height (2013–2017, entire basin), leaf area index (LAI, 2013–2015, midstream and downstream), biomass (2013–2014, midstream), photosynthesis (2014, downstream), and soil respiration (2014, downstream) were investigated by regular manual observation during 2013 to 2017. In addition, automatic observation devices for monitoring phenology, FVC, and LAI were installed and have been operational at three superstations since June 2018.

Runoff and Groundwater Table

Eight hydrographic sections were established in the main channel of the midstream region from June 2012 to December 2015 along with three hydrological stations. Instruments including an acoustic Doppler current profiler and an ultrasonic water level meter are used to monitor runoff (water discharge and water level). Based on these measurements, dynamic changes in the river flow in each section were monitored in the midstream region. In addition, since June 2014, five systems for groundwater table measurement have operated in the downstream region, near Sidaoqiao, Mixed Forest, *Populus euphratica*, Cropland, and Barren Land stations. In April 2016, temperature and moisture sensors were installed under and between the *Populus euphratica* trees (2, 4, 10, 20, 40, 60, 100, 160, 200, and 240 cm) in the downstream region.

Other Parameters

In 2012, soil parameters (including soil texture, porosity, bulk density, saturated water conductivity, and soil organic matter) were measured at each station in the midstream region and at the Arou superstation in the upstream region.

During the period 2013 to 2016, measurements were made of spectral reflectance (2014, downstream), surface emissivity (2014–2015, typical land surfaces across the entire basin), microwave radiation characteristics (2013, midstream and upstream), and component temperature (2014–2016, downstream). A fluorescent spectrum automatic observation system has been operating at the Daman superstation since May 2017 to monitor the reflectance spectra and chlorophyll fluorescence.

Eco-hydrological Wireless Sensor Network

There are three categories of wireless sensor networks: (i) installed in the LAS source area in the hydrometeorological observatory to provide basic data for the ET study (Arou and Daman superstations, WSN1, see above); (ii) installed in the dedicated campaigns and experiment in 2012 to validate the airborne, medium- and high-resolution satellite remote sensing products (kernel matrix in midstream, WSN2, see below); and (iii) installed for long-term observations (in the upstream region, WSN3, described here).

To analyze the spatiotemporal distribution and dynamic characteristics of soil moisture and to validate microwave soil moisture products in upstream regions, a WSN consisting of 40 nodes was established from June to August in 2013 to monitor soil moisture and temperature (4, 10, and 20 cm), land surface temperature, snow depth, and precipitation under alpine meadow, cropland, and bare land surfaces (WSN3; Jin et al., 2014; Kang et al., 2017). The region, named the Babao River (the region outlined in red in Fig. 2), is a sub-basin upstream of the HRB. The node distribution was optimized based on a spatial sampling strategy (Fig. 5). There are three categories of nodes equipped with different sensors: (i) soil moisture and temperature (21 nodes); (ii) soil moisture, temperature, and land surface temperature (8 nodes); and (iii) soil moisture, temperature, land surface temperature, snow depth, and precipitation (11 nodes).

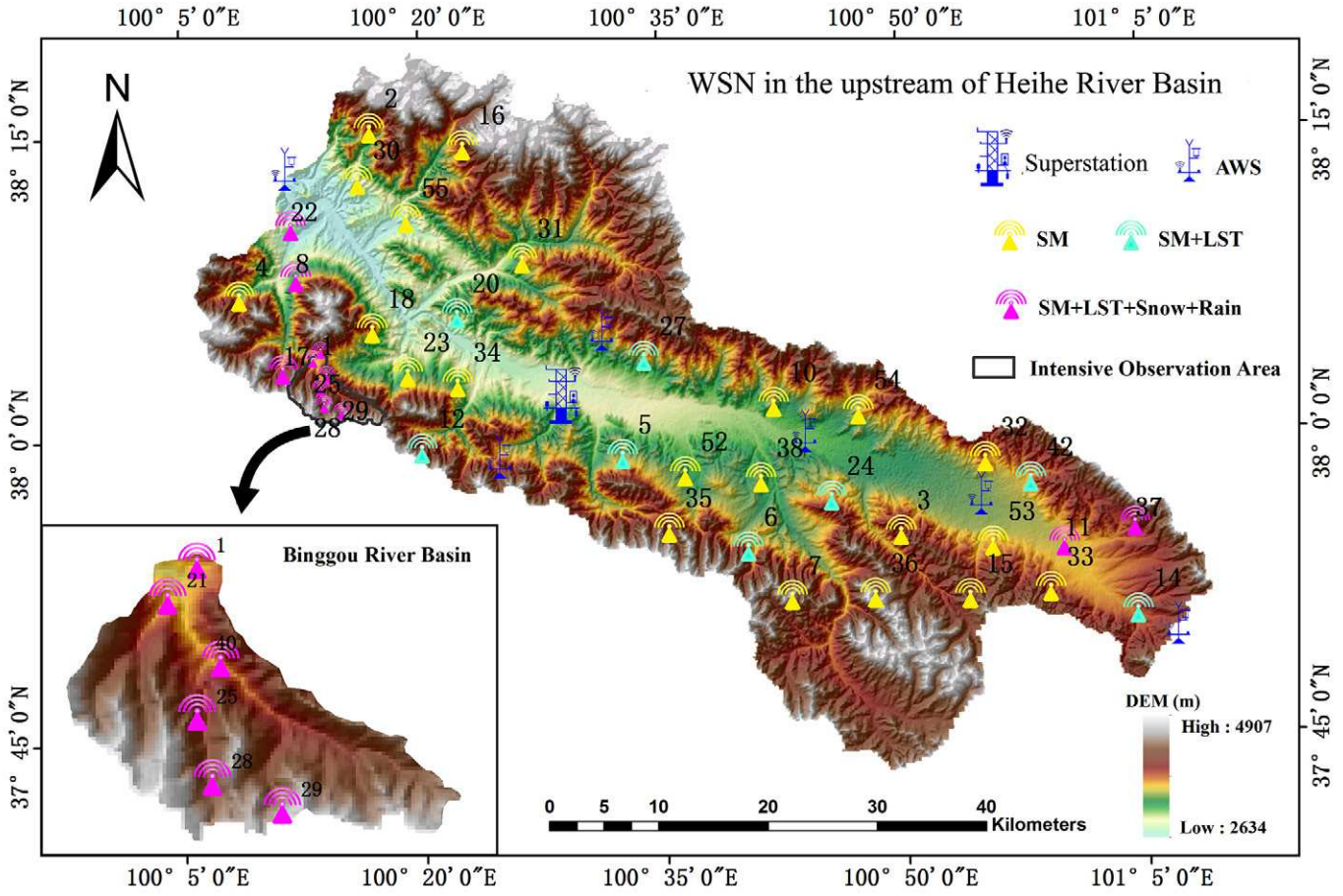

Fig. 5. The wireless sensor network in the upstream region (WSN3), superimposed on a digital elevation model (DEM), showing the locations of the superstation, automatic weather stations (AWS), soil moisture (SM), and land surface temperature (LST) monitors.

Satellite Remote Sensing Products

Currently, the spatial resolution of most remote sensing products is coarser than 1 km, and they have a temporal resolution of 8 d, 16 d, or longer at the global scale. The surface heterogeneity is increased at the watershed scale because of the complicated terrain and fragmented landscapes. In addition, an inland river basin presents a diverse set of landscape types, with dramatic changes in the water cycle and ecological process. Thus, remote sensing products with high precision and high spatial and temporal resolutions are urgently needed in the HRB. Based on multi-source remote sensing technologies and datasets over the HRB, nine remote sensing products for key land surface variables were developed with higher spatial and temporal resolution, such as land use/cover (30 m monthly, 2011–2015; Zhong et al., 2015), phenology (1 km, 2012–2015; Zhong et al., 2015), FVC (1 km every 5 d, 250 m every 16 d, 30 m monthly, 2011–2015; Mu et al., 2015), net primary productivity (1 km every 5 d, 2012–2015; Zhong et al., 2015), LAI (1 km every 5 d, 2010–2015; 30 m monthly, 2010–2015; Liao et al., 2013), snow cover (0.5 km daily, 2000–2015; Zhang et al., 2014), soil moisture (1 km daily, 2008–2015; Kang et al., 2017), precipitation (0.05° hourly, 2000–2016; Pan et al., 2012, 2015), and ET (ETMonitor, 1 km daily, 2008–2016; ETWatch, 1 km monthly, 2000–2014; Hu and Jia, 2015).

Dedicated Campaigns and Experiments

The dedicated campaigns and experiments include the Multi-Scale Observation Experiment on Evapotranspiration over Heterogeneous Land Surfaces (HiWATER-MUSOEXE) and the airborne remote sensing experiment, which are simultaneous airborne, satellite-borne, and ground-based experiments that were mainly conducted in 2012 (part of the airborne remote sensing experiment was conducted in 2014).

The HiWATER-MUSOEXE

The HiWATER-MUSOEXE was conducted in the midstream region of the HRB between 3 May and 21 Sept. 2012 and involved a flux observation matrix, wireless sensor network (WSN2), and auxiliary parameter observations.

Two nested matrices were involved in the HiWATER-MUSOEXE: one large matrix (30 by 30 km) and one kernel matrix (5.5 by 5.5 km) (Fig. 6a). The large matrix contained one superstation (no. 15, Daman superstation) and four ordinary stations around the oasis (desert, desert steppe, Gobi, and wetland surfaces). The kernel matrix was located in the Yingke and Daman irrigation

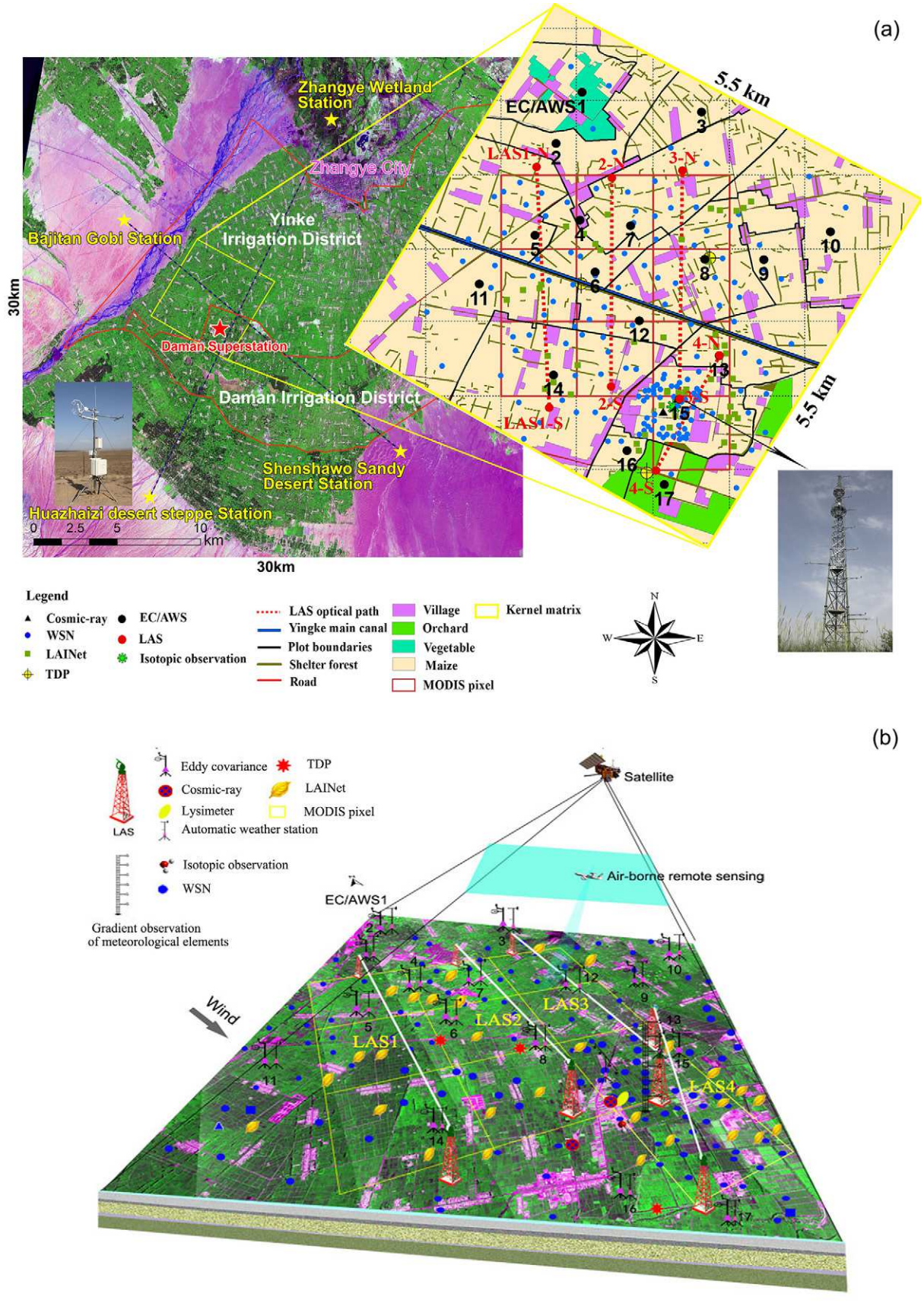

Fig. 6. Flux observation matrix: (a) two nested matrices, including the large matrix (30 by 30 km) and the kernel matrix (5.5 by 5.5 km); and (b) the kernel matrix (WSN, wireless sensor network; LAINet, a wireless leaf area index sensor network; TDP, thermal dissipation probe; EC/AWS, eddy covariance and automatic weather station; LAS, large aperture scintillometer).

district, and the main land surfaces comprised maize, residential areas, vegetables, and orchards. These characteristics represented the major land cover and plant structures in the oasis in the midstream region of the HRB.

The kernel matrix was initially divided into 17 sample plots according to the distributions of crops, shelterbelts, residential areas, roads, and canals, as well as soil moisture and irrigation status. In total, the sample area included one residential area station, one orchard station, one vegetation station, and 14 maize stations. At Station 15 (Daman superstation), there were two EC sets and seven layers in the meteorological gradient observation system used to obtain surface fluxes and meteorological elements at different heights. In addition to Station 15, there was one EC system and one automatic weather station at each station to observe surface fluxes and meteorological elements at each plot (Liu et al., 2016). Moreover, transpiration from shelterbelts at different heights and diameters at breast height were measured using a thermal dissipation probe around Stations 6, 8, and 17 (three poplar trees in each station were equipped with three thermal dissipation probes at a height of 1.3 m), which represented the mean transpiration conditions of the shelterbelt forest (Qiao et al., 2015). There were also four groups of near-infrared LASs (with eight sets) within the kernel matrix (three groups were in three 3 × 1 MODIS pixels, named LAS1 through LAS3 from west to east, respectively; one group was in one 2 × 1 MODIS pixel, named LAS4) to measure sensible and latent heat flux at the pixel scale. In addition, two cosmic-ray probe observations (Zhu et al., 2015) and in situ measurements of the isotopic composition of atmospheric water vapor (partitioning ET into evaporation E and transpiration T) (Wen et al., 2016) were conducted near Station 15 (Fig. 6b). The kernel matrix included a WSN (WSN2, Fig. 6a and 6b) that was active from May to September 2012, with 180 soil moisture and temperature nodes (Jin et al., 2014) and 42 LAI nodes (Qu et al., 2014).

Several auxiliary parameters in the kernel and large matrix areas were measured during the HiWATER-MUSOEXE in 2012. These auxiliary parameters can be divided into three categories: airborne sensor calibration parameters (GPS sounding, differential GPS, ground synchronous observations, aerosol optical depth, air temperature and wind speed profile observed by wind profile radar, and conventional radiosonde sounding observations), ground-based remote sensing parameters (the bidirectional reflectance distribution function, spectral reflectance, and emissivity), and ground auxiliary parameters (vegetation and soil parameters and field management and irrigation information) (Fig. 7).

Airborne Remote Sensing Experiments

The airborne remote sensing experiments were performed successively in 2012 and 2014 during the HiWATER experiment and involved 21 mission flights (>100 flying hours). A total of 24 categories of raw data and 19 categories of airborne remote sensing products were acquired that provided high-spatial-resolution land surface information.

There were a total of 17 missions during approximately 81 flight hours by Y-12 multipurpose transport aircraft during the period of 22 May to 28 Aug. 2012. The payloads on the flights over the upstream and midstream regions included a hyperspectral imager (thermal airborne spectrographic imager and compact airborne spectral imager), a multi-angle thermal infrared imager (wide-angle infrared dual-mode line/area array scanner, WiDAS), lidar (Leica ALS70), a high-resolution charge-coupled device (CCD, Phase iXA), and a microwave radiometer (Polarimetric L-band Multibeam Radiometer) (Fan et al., 2015). Parameters such as the land surface temperature, albedo, planting structure, LAI, canopy height, digital elevation model, digital surface model, and soil moisture were retrieved (Table 2). Overall, multiresolution, multi-angular, and multispectral airborne data were obtained via the airborne remote sensing experiment. These data are particularly useful in developing and validating scaling methods and remote sensing models (Li et al., 2017a).

In addition, flights with lidar, a hyperspectral imager (AISA Eagle II), CCD, and thermal imager were conducted in the core area of the Ejin Banner oasis in the downstream region, while supplementary lidar and CCD measurements were conducted in Hulugou in the upstream region from 29 July to 5 Oct. 2014 (Table 2).

Data Quality Control

Data quality control is a last-forever process in the Heihe Integrated Observatory Network. A series of quality control measures were undertaken and implemented primarily through the following procedures: intercomparison and calibration of experimental instruments, observatory maintenance, and data processing.

Intercomparison and Calibration of Experimental Instruments

Sensor intercomparisons and calibrations, such as surface energy flux instruments (e.g., EC system, LAS, and radiometers), meteorological sensors, and soil moisture sensors are prerequisites to ensure data quality in the Heihe Integrated Observatory Network.

Prior to implementing the flux observation matrix in the midstream region and the installation of the hydrometeorological instruments in the upstream and midstream regions, an instrument intercomparison experiment was performed. The area selected for the intercomparison campaign was located in the Bajitan Gobi Desert (no. 17 in Fig. 2, west of Zhangye city [100.30° E; 38.91° N]). The Bajitan Gobi Desert is a nearly flat, open land surface that is covered with coarse-grain sand and small pebbles with withered sparse scrub vegetation. The intercomparison experiment was performed from 14 to 24 May2012, and the selected study area was 300 by 600 m. Seven LAS groups were located along the north and south sides of the area, while 20 EC sets and 18 radiometer sets were located in the central area of the region. The results showed that the instruments were consistent with each other, with differences (i.e., regression slopes) of 3 and 10% for sensible heat flux and latent heat flux (EC), respectively. A 2% difference was found for sensible heat flux (LAS), and <1% difference was found for net radiation. The EC and LAS

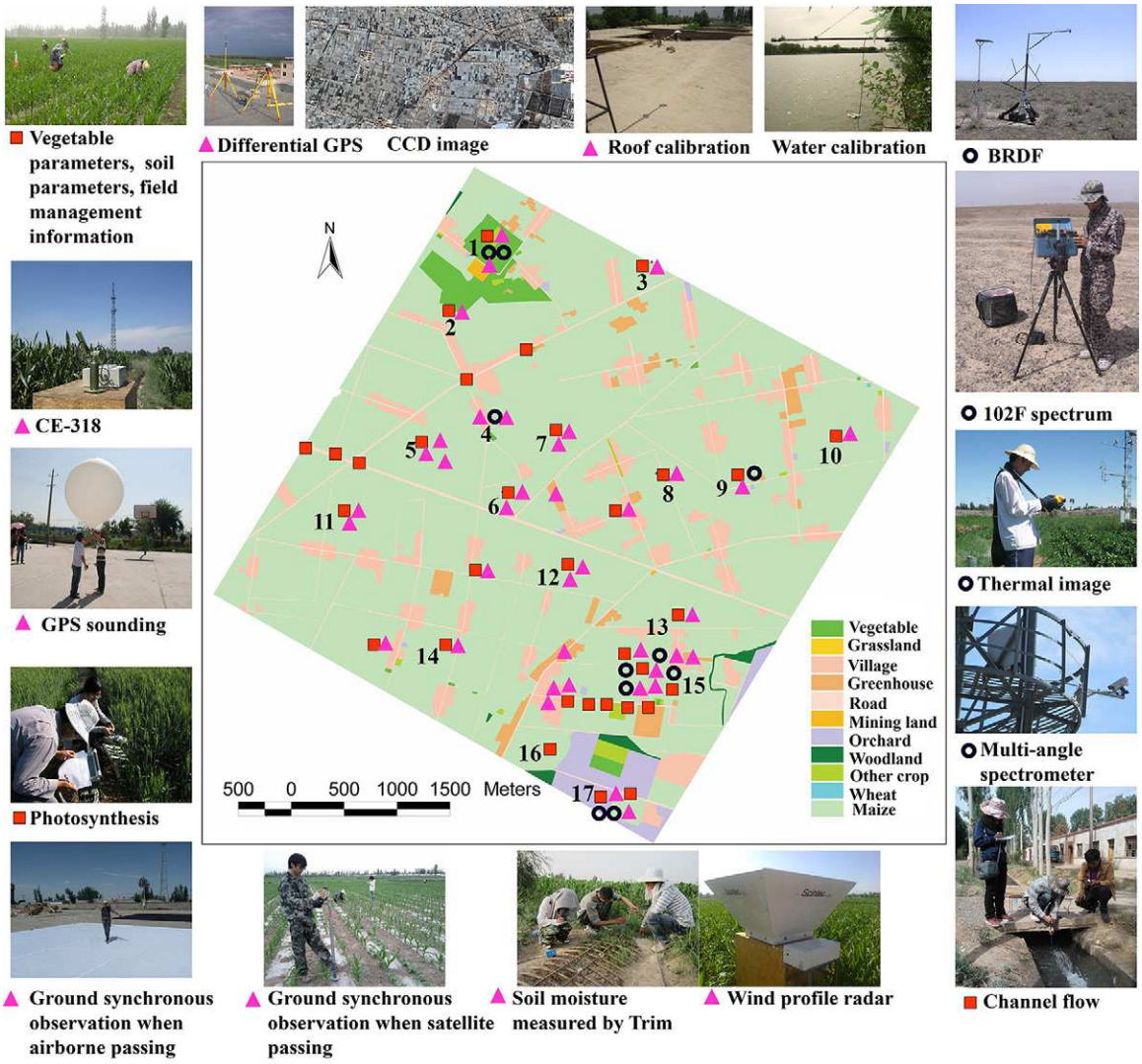

Fig. 7. Auxiliary parameter observations (pink triangles: airborne sensor calibration parameters; black circles: ground-based remote sensing parameters; red squares: ground auxiliary parameters). BRDF is the bidirectional reflectance distribution function.

measurements were consistent with a regression slope of approximately 3%, which demonstrated the reliability of the measured data. More details can be found in Xu et al. (2013) and Liu et al. (2016).

Prior to the installation of the hydrometeorological instruments in the downstream region, another intercomparison experiment was conducted in a relatively homogeneous shrub region around the Ejin Banner oasis (101.07° E, 41.92° N) from 27 June to 3 July 2013. This intercomparison experiment involved two LASs, six EC systems, and six radiometers. The regression slopes of the EC systems were 3 and 7% for sensible heat and latent heat flux, respectively. A 3% difference was found for sensible heat flux (LAS), and <1% difference was found for net radiation. The EC and LAS measurements were comparable to a regression slope of approximately 7%. The results of our intercomparison are better than those reported for the FIFE and the Energy Balance Experiment (EBEX-2000) comparisons (Nie et al., 1992; Mauder et al., 2007).

In addition, comprehensive calibration and intercomparison of the instruments are undertaken regularly, including in the spring and autumn (i.e., before and after the plant growing season) for the infrared gas analyzer sensor of the EC system. In addition, air temperature and humidity and wind speed sensors in the multilayers for gradient observation systems are compared at the same height prior to installation, and rain gauges of different types are compared in a field experimental area in the upstream and midstream regions. Prior to installation, soil moisture probes are calibrated in dry and wet soils and infrared radiation temperature sensors are calibrated using a blackbody source. All these intercomparisons and calibrations help ensure data quality, which is helpful for instrument placement and subsequent data analyses, too.

Observatory Maintenance

The data of the Heihe Integrated Observatory Network are transferred to a data management and control system in real time

Table 2. Airborne data information.

Area	Flight time	Sensor†	Target‡
Large matrix in the midstream area	30 June 2012	TASI + PLMR	land surface temperature
	10 July 2012	TASI + PLMR	
	4 Aug. 2012	WIDAS + PLMR	
Kernel matrix in the midstream area	29 June and 8 July 2012	CASI + PLMR	vegetation classification, physiological and biochemical parameters
	26 July and 4 Aug. 2012	WIDAS + PLMR	component temperature, albedo, classification
	25 July 2012	ALS70 lidar	canopy height, planting structure
Midstream area	3 July and 4 July 2012	TASI + PLMR	water body distribution
Midstream area	29 June 2012	CASI + PLMR	surface cover
Upstream area	2 Aug. 2012	WIDAS + PLMR	soil moisture, land surface temperature, classification
Upstream area	25 July, 19 Aug., 25 Aug., and 28 Aug. 2012	ALS70 lidar	DEM, DSM
Ejin Banner oasis in the downstream area	29 July and 4 Aug. 2014	AISA Eagle II	vegetation parameters, land surface temperature, classification
Ejin Banner oasis in the downstream area	29 July and 4 Aug. 2014	lidar + CCD	DEM, DSM
Upstream area	23 Sept. and 5 Oct. 2014	lidar + CCD	DEM, DSM

† CASI, Compact Airborne Spectral Imager; CCD, charge-coupled device; TASI, thermal airborne spectrographic imager; PLMR, Polarimetric L-band Multibeam Radiometer.
‡ DEM, digital elevation model; DSM, digital surface model.

through a wireless transmission mode. The system includes automatic data collection, data storage and management, automatic data quality check, real-time data visualization, and instrument status monitoring (Fig. 8).

A maintenance process is strictly followed to ensure the quality of the observation data. In general, the routine maintenance processes for the Heihe Integrated Observatory Network include four steps: daily, 10 d, monthly, and annually (Fig. 9). Each day, the real-time data in the observatory are received by the wireless transmission mode to check data integrity and monitor instrument status. Every 10 d, the time series of each observed element at every station is plotted automatically using the data management and control system. The data quality can be further examined by checking the time series plot. Each month the engineers visit every station for routine inspection, including manual data collection, sensor checking, cleaning the sensors that are easily affected by external environmental elements (e.g., four-component radiation and the CO_2–H_2O infrared gas analyzer), taking pictures of the underlying surface and surrounding environment, measuring the plant height, recording the phenology, and writing an inspection logbook. Annually the engineers preprocess and check the data for the entire year. During the routine maintenance, if any problems

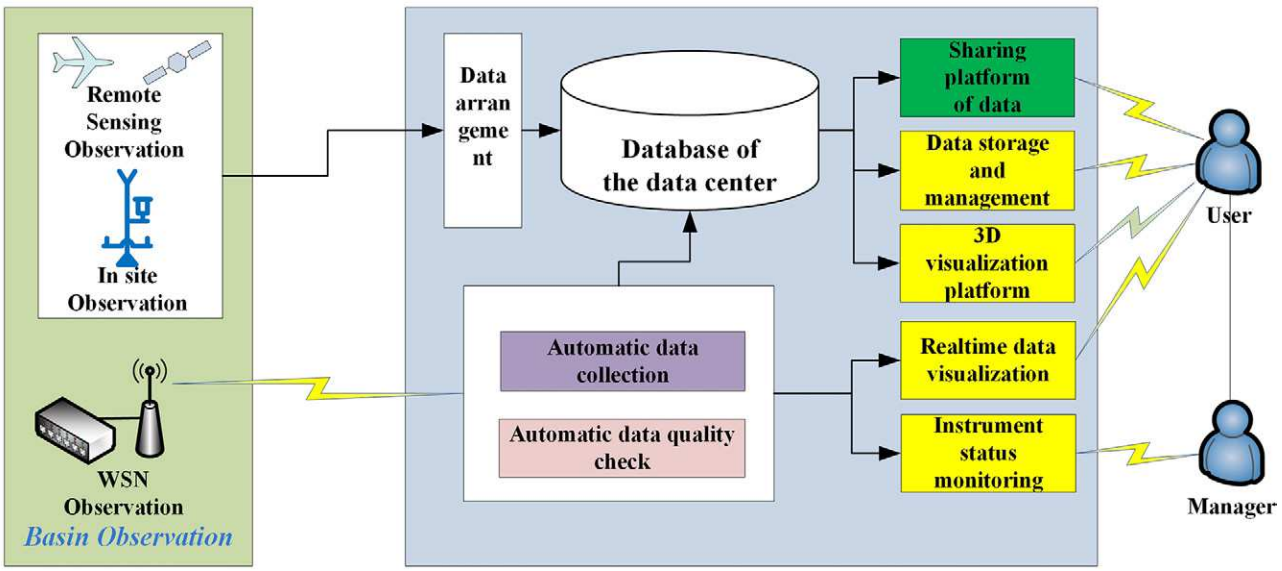

Fig. 8. Data management and control system for the remote sensing, on-site, and wireless sensor (WSN) networks.

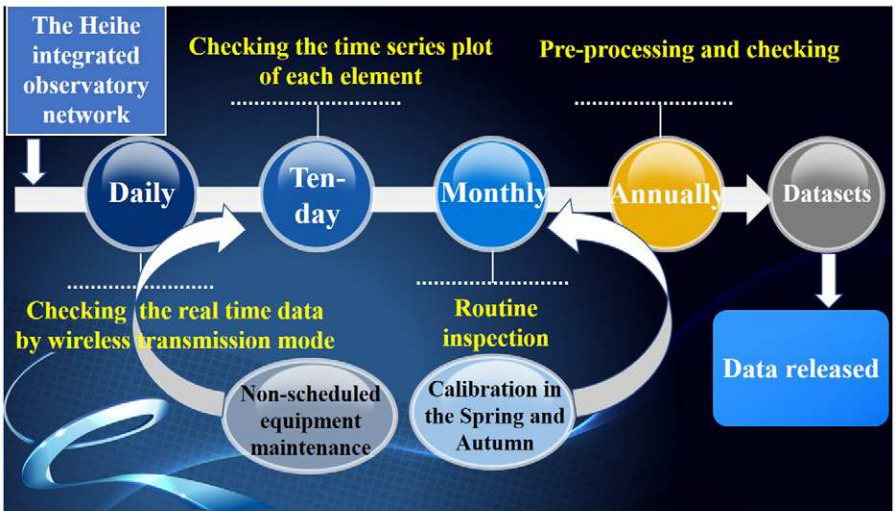

Fig. 9. Flow chart of observatory maintenance.

are found, we visit this station specifically to repair and replace those sensors.

Data Processing

A complete and standard data post-processing procedure was developed for different types of observation data, including surface fluxes and hydrometeorological data (Liu et al., 2011, 2013), WSN data, ground auxiliary parameters (Jin et al., 2014), etc., and careful data post-processing and checking are performed accordingly.

First, a detailed data processing scheme is formulated for the different data sets, and careful data processing and screening are performed. Second, data quality self-examination, cross-check, and expert review are applied. Finally, the metadata for each dataset are written including station descriptions, processing steps, notices, references, and projects. After these steps are completed, the processed datasets and the metadata are released on the website (Fig. 10).

Data Management and Sharing

Under an open data policy, all the data are released freely on the Chinese version of the website (http://www.heihedata.org and http://westdc.westgis.ac.cn) and the English version of the website (http://card.westgis.ac.cn) (Li et al., 2017a). By the end of 2017, 783 Chinese and 514 English datasets had been released. These data were browsed approximately 4,820,000 times and downloaded more than 10,000 times. The total amount of data exceeded 21.7 TB and were used to serve more than 400 research projects. Based on these released data, 716 articles have been published, including 498 Science Citation Index journal articles.

New Insights and Novel Scientific Findings

Progress has been made based on the Heihe Integrated Observatory Network in a number of areas, including observed

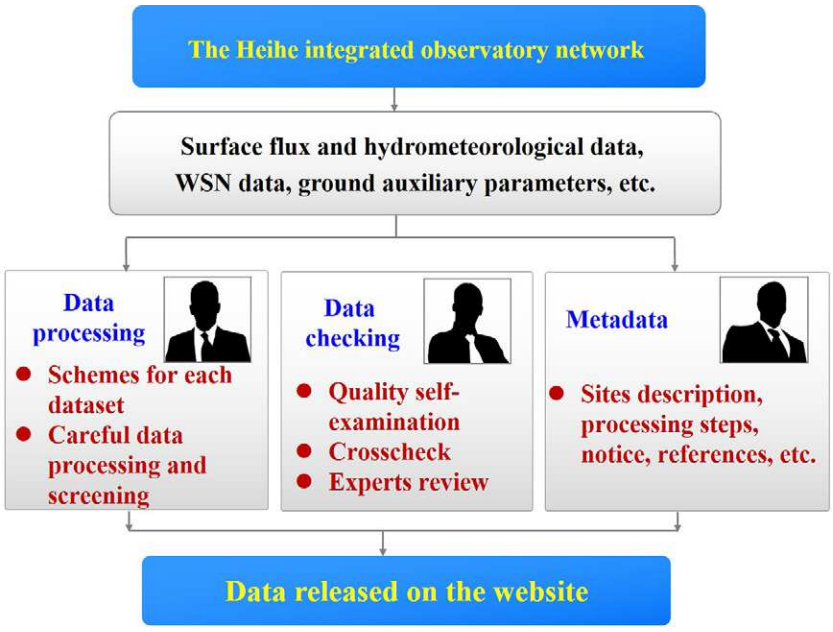

Fig. 10. Data processing chart.

trends, scaling methods, high-spatiotemporal-resolution remote sensing products, and model–data integration, basically achieving the goals of the Heihe Integrated Observatory Network. Taking the ET as an example, new insights and novel scientific findings have been introduced from these four aspects as described below.

The Trend of Evapotranspiration and Its Partitioning

There are currently approximately 10 yr of ET and related environmental element observations available in the HRB. Based on the HRB dataset, many studies have been conducted on the trend of ET and its partitioning. Liu et al. (2011) investigated the seasonal variations of energy fluxes at three sites (no. 5, 10, 16 in Fig. 2), found an obvious "oasis effect" in the midstream irrigated cropland, and also gave the reasons for the difference between EC and LAS measurements, namely the energy imbalance phenomenon of EC observations, the heterogeneity of the underlying surfaces, and the difference between the source areas of the LAS and EC measurements. In addition, the energy balance closure of the EC was evaluated at all stations in the HRB at a range of 0.7 to 1.0, which is consistent with previous studies (Li et al., 2016; Xu et al., 2017a; Zhou et al., 2018b). Due to the unique and diverse landscapes, ET differs significantly among the upstream, midstream, and downstream regions, with annual ET values that range from 43 to 1057 mm. Unsurprisingly, the ET values are largest in summer (July or August) and lowest in winter. Figure 11 shows the variations in ET and related environmental elements at three superstations from 2008 to 2017. The range of annual ET is 430 to 590 mm in the alpine meadow at the Arou superstation, 550 to 700 mm in irrigated cropland at the Daman superstation, and 540 to 680 mm in riparian forest at the Sidaoqiao superstation. There is no obvious trend in ET interannual variations at the Arou and Sidaoqiao superstations; however, a decreasing trend of annual ET since 2016 can be seen at the Daman superstation due to changes in irrigation methods (from flooding irrigation to drip irrigation).

Based on in situ measurements of the isotopic compositions of atmospheric water vapor via a cavity ring-down spectroscopy water vapor isotope analyzer at two heights above the canopy during the maize growing season in the midstream region (Daman superstation) of the HRB in 2012, Huang and Wen (2014) determined the isotopic composition of ET via the gradient method. Combined with the observed water and energy fluxes and the isotopic measurements dataset at this station, Wen et al. (2016) partitioned the ET into T and E via an isotopic approach using a steady-state assumption. The relative contribution of transpiration to evapotranspiration (T/ET)

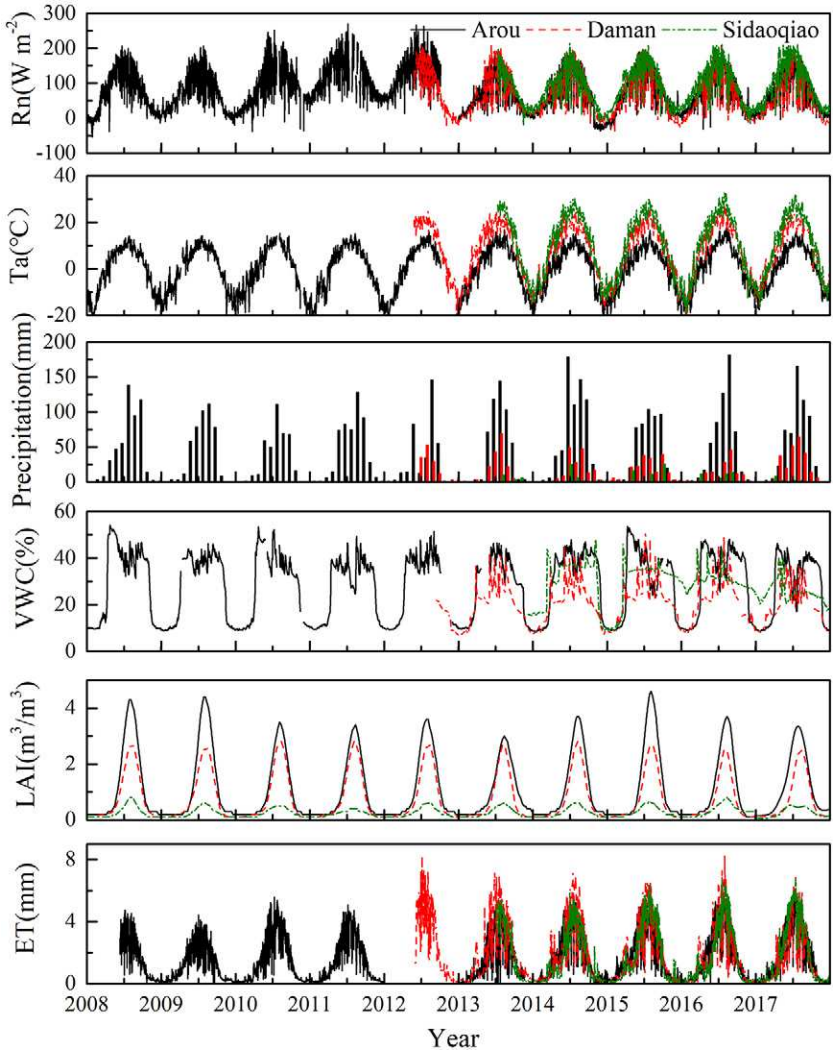

Fig. 11. The variations of evapotranspiration (ET), leaf area index (LAI), volumetric water content (VWC), precipitation, air temperature (T_a), and net radiation (R_n) at three superstations (2008–2017).

ranged from 0.71 to 0.96 with a mean of 0.87 ± 0.052 for the growing season, which was in good agreement with the mini-lysimeter measurements that showed a mean *T*/ET of 0.86 ± 0.058.

Wang et al. (2016) used a Soil–Plant–Atmosphere Continuum with Isotope Tracer (Iso-SPAC) model to reproduce the dynamics of the isotope composition of ET and further verify the validity of the steady-state assumption, which could be reasonably used to evaluate the seasonal variations in isotopic composition of *T* and ET partitioning. Based on continuous observations of the EC dataset, Zhou et al. (2018a) partitioned ET across three typical ecosystems in the upper (alpine meadow), middle (irrigated cropland), and lower (*Populus euphratica*) reaches of the HRB based on the concept of underlying water use efficiency (uWUE). The uWUE method showed good agreement when compared with the stable isotope method and the sap flow–EC method. The uWUE method was further verified in comparison with the stable isotope method, mini-lysimeter–EC method, and sap flow–EC method based on multiyear observed EC and automatic weather station observation dataset in other ecosystems. The *T*/ET ratio was estimated across six typical ecosystems in the upper (alpine meadow and Qinghai spruce), middle (maize and *Kalidium foliatum* desert) and lower reaches (*Tamarix* and *Populus euphratica*) of the HRB during the growing season from 2012 to 2016, and the controlling factors affecting the divergence of *T*/ET in these six typical ecosystems were investigated. The average *T*/ET results for these six ecosystems during the multiyear growing season were 0.53 (alpine meadow), 0.59 (maize), 0.37 (*Kalidium foliatum* desert), 0.56 (*Tamarix*), and 0.60 (*Populus euphratica*) from 2012 to 2016 and 0.52 (Qinghai spruce) from 2008 to 2010.

Developing Scaling Methods

The multiscale observations in the HRB provide a unique opportunity to support the development and improvement of scaling methods for ET, soil moisture, LAI, and other land surface parameters (Ran et al., 2016; Jin et al., 2017).

Studies on ET upscaling methods have been investigated based on a flux observation matrix and airborne and satellite-based remote sensors. Ge et al. (2015) used the normalized difference vegetation index, land surface temperature (LST), FVC, and wind speed as auxiliary information, and the area-to-area regression kriging (ATARK) method was used to upscale the sensible heat flux (*H*) from the EC scale to the LAS scale. However, this method did not consider the path-weighting function in the EC to LAS scale kriging with regression residuals. Thus, Hu et al. (2015) developed the weighted area-to-area regression kriging (WATARK) based on ATARK and upscaled *H* on the EC scale to that on the LAS scale. The results showed that the WATARK method performed better than the area-weighted (AW), footprint-weighted, multiple linear regression, and ATARK methods. Liu et al. (2016) proposed an upscaling method (i.e., the integrated Priestley–Taylor equation) to acquire ET at the satellite pixel scale. Finally, a combined method (i.e., applying the AW method to relatively homogeneous surfaces or otherwise using the Priestley–Taylor method) was proposed to acquire both instantaneous and daily "ground-truth" ET data at the satellite pixel scale. Xu et al. (2017b) applied the AW method and combined it with a footprint analysis and the multivariate regression method to upscale multisite EC flux data in the kernel matrix area of the HiWATER-MUSOEXE. To determine the most appropriate upscaling approach for acquiring ground-truth ET data at the satellite pixel scale, Li et al. (2018a) used the dataset from two flux observation matrices in the midstream and downstream regions of the HRB and compared six upscaling methods (AW, Priestley–Taylor, WATARK, artificial neural network, Random Forest, and a deep belief network) via direct validation and cross-validation. Finally, an optimized method (using the AW and WATARK methods for homogeneous and moderately heterogeneous land surfaces, respectively, and using the Random Forest method for highly heterogeneous land surfaces) was proposed to acquire daily "ground-truth" ET data at the satellite pixel scale, which were used to validate remotely sensed ET products. Xu et al. (2018) upscaled ET from flux towers to the regional scale based on ground measurements from 36 EC observation sites (65 site years) across the HRB using five machine learning methods. The gridded ET over the watershed scale (defined as ETMap) was generated at a spatial resolution of 1 by 1 km for each day. The ET from the ETMap captured the spatial and temporal patterns of ET at the regional scale.

Mapping High-Spatiotemporal-Resolution Evapotranspiration and Its Components with Remote Sensing Data

Data fusion approaches offer a feasible and inexpensive way to reconstruct land surface dynamics at a high spatiotemporal resolution using remote sensing data from both finer and coarser resolution sensors. Li et al. (2017b) proposed an approach to estimate instantaneous and daily 90-m ET during the growing season (June–September) over the midstream oasis of the HRB using the Surface Energy Balance System (SEBS) by fusing MODIS and Advanced Spaceborne Thermal Emission and Reflection Radiometer (ASTER) data using the Spatial and Temporal Adaptive Reflectance Fusion Model (STARFM). The estimated ET agreed well with the EC measurements during the HiWATER-MUSOEXE. Ma et al. (2018) proposed a scheme to estimate daily ET over the oasis irrigation area of the HRB at a Landsat-like scale (100 m) using the enhanced STARFM and a revised SEBS model, where the parameters at the Landsat-like scale were obtained by fusing data from MODIS and the Landsat Enhanced Thematic Mapper Plus (ETM+). Low mean absolute percentage errors and root mean square errors compared with EC measurements indicated that the estimation scheme successfully predicted the fine spatiotemporal distribution of ET. Additionally, this study compared the input parameter fusion approach with the ET fusion approach; the results suggested that the input parameter fusion approach performed better over heterogeneous surfaces. Moreover, this daily ET dataset was used to assess irrigation water efficiency at the irrigation district and village scales, knowledge of which can help improve irrigation decisions and optimize water resource management in the HRB.

Meanwhile, the Heihe Integrated Observatory Network provided an opportunity to investigate estimation of *E* and *T* from site to river basin scales (Xiong et al., 2015; Yang et al., 2015a; Song et al., 2016a; Xu et al., 2016; Yao et al., 2017b; Song et al., 2018). At the site scale, Xu et al. (2016) partitioned ET into *E* and *T* with a two-source variational data assimilation scheme (TVDA). The TVDA was compared with the two-source energy balance model (TSEB) and accomplished via EC measurements and stable isotope measurements at the Daman superstation. The results showed that the accuracy from TVDA was comparable to that of the TSEB model when using ground-measured LST data as the model inputs, while the TVDA outperformed TSEB when using noisy LST as the model inputs. At the field scale, a refinement of the TSEB (TSEB-A) was developed using a non-iterative approach based on the application of the Priestley-Taylor formulation for partitioning surface temperature and estimating soil evaporation from soil moisture observations under advective conditions. The TSEB-A model improved the estimation of ET and its *E* and *T* components by comparing the data with EC measurements and stable isotope measurements at the Daman superstation (Song et al., 2016a). At the regional scale, the soil and vegetation component temperature derived from ASTER image data were used as model inputs ($TSEB_{CT}$). The $TSEB_{CT}$ model outputs of sensible and latent heat fluxes were in closer agreement with the observations and were generally found to be more robust in component flux estimation than the $TSEB_{PT}$ (which used composite surface temperatures as model inputs) under a heterogeneous advective environment (Song et al., 2016b). Finally, multiyear remote sensing of all-weather daily ET, *E*, and *T* were produced using the MODIS-based dual temperature differences model under different land covers (where areas of sparse vegetation and bare land account for approximately 83.5% of the entire river basin) in the HRB. The ET, *E*, and *T* during the growing season are approximately141.4, 93.9, and 47.5 mm, respectively, in the HRB (Fig. 12). The remotely sensed ET product had mean absolute deviation percentage errors of only approximately 20% during the growing season under clear sky conditions. Moreover, spatially and temporally continuous daily *E* and *T* at the river basin scale proved useful in developing a sustainable water resource strategy (Song et al., 2018).

Quantifying the Hydrological Cycle in the Heihe River Basin

Significant challenges remain in quantitative understanding of the hydrological cycle in endorheic basins due to poor data availability and inadequate methods. To address these challenges, we performed a series of studies to assess the water resources by establishing an integrated modeling system in the HRB.

For the upstream cold region in the HRB, a distributed cold region model (the Geomorphology-Based Ecohydrological Model, GBEHM) was developed to simulate hydrological processes in the cryosphere, including snowmelt, frozen–thawed soil, glacier changes, and discharges (Yang et al., 2015b; Gao et al., 2018). For the middle and lower reaches of the basin, which include oasis and broad desert regions, an eco-hydrological model named Hydrological-Ecological Integrated Watershed-Scale Flow (HEIFLOW) was developed to simulate irrigation water balances,

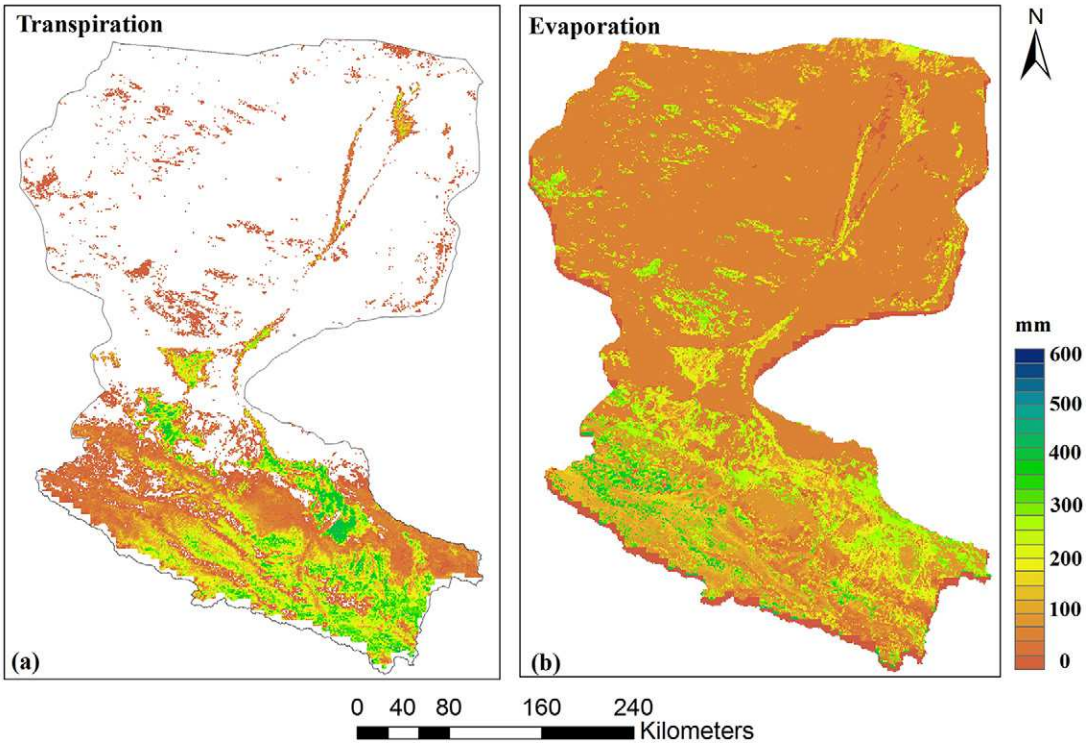

Fig. 12. Spatial distributions of growing season (June–September) (a) transpiration and (b) evaporation in the Heihe River Basin (2012–2015, 1-km resolution).

two-dimensional overland flow and river channel hydrodynamics, and the growth of agricultural crops and desert vegetation (Tian et al., 2015). The GBEHM and HEIFLOW were coupled together to simulate the water balance in the HRB after overcoming a series of challenges, including correcting bias due to wind-influenced precipitation, improving the turbulent flux parameterization under water-stressed conditions, upscaling the ET components to improve irrigation efficiency calculations, and distinguishing the complex eco-hydrological roles of vegetation at the microscale across deserts and grasslands. The forcing data were derived from a dynamic downscaling dataset using the Weather Research and Forecasting model and the Regional Integrated Environmental Model System (Li et al., 2018b). More suitable land cover maps were reproduced for the integrated simulation based on remote sensing data acquired in the 2000s. To validate and calibrate the modeling system, abundant and unique observation data from the Heihe Integrated Observatory Network were adopted, including time series of observed discharges and the groundwater table in the HRB, in situ and remote sensing measurements of ET, and other site observations such as soil moisture and temperature profiles. The magnitudes of surface water withdrawal and groundwater extraction, which are necessary in the modeling system, were derived from a statistical dataset via the local water authorities (Li et al., 2018b).

A comprehensive and quantitative estimation of water balances across different landscapes were determined in the HRB for the first time (Fig. 13), and it updated our understanding of the cryosphere contribution in this typical endorheic basin. The results indicate that rainfall, snowmelt, and glacier melt contribute approximately 71, 25, and 4%, respectively, to the total runoff. The ET from the upper reaches is 5.54×10^9 m^3 yr^{-1}. In the middle and lower reaches, we confirmed the distribution of available water across different landscapes. The results indicate that in the midstream region, irrigation water withdrawal amounts to 2.40×10^9 m^3 yr^{-1}, of which 78.2% is withdrawn from the Heihe and Liyuan rivers. The ET from this region is 4.28×10^9 m^3 yr^{-1}. In the downstream region, approximately 39% of the available water is used in natural oases, 4% contribute to the terminal lake, 9% is used to maintain the stream flow and reservoirs, 13% is used for irrigation, and approximately 35% evaporates in the desert (Li et al., 2018b). The total ET from the downstream region is 5.69×10^9 m^3 yr^{-1}.

Our results also indicated a series of scientific findings in the endorheic basin. We found that precipitation, runoff, snowmelt, and glacier melt increased continuously in the upstream area of the HRB from 2001 to 2012 under a warming climate (Li et al., 2018b). The melting of frozen soil contributed significantly to the increased baseflow in the total runoff (Gao et al., 2018). We found that the maximum water use for the midstream agricultural area had been reached, which indicates that groundwater overuse has already become a serious problem (Li et al., 2018b).

Future Perspectives

Under the framework of the WATER and HiWATER experiments, a state-of-the-art and intensive flux observation matrix has been developed, and a multi-element, multiscale, networked, and expanded integrated watershed observatory has been established. Several key scientific issues, such as spatial heterogeneity, scaling, and uncertainty, were explored. Furthermore, the comprehensive monitoring capacity of land surface processes was improved, which helps with the integrated river basin management. The Heihe Integrated Observatory Network has been operating since 2007, and all the data have been released under a data sharing policy. Series of achievements, such as observed trend, scaling methods, high spatiotemporal

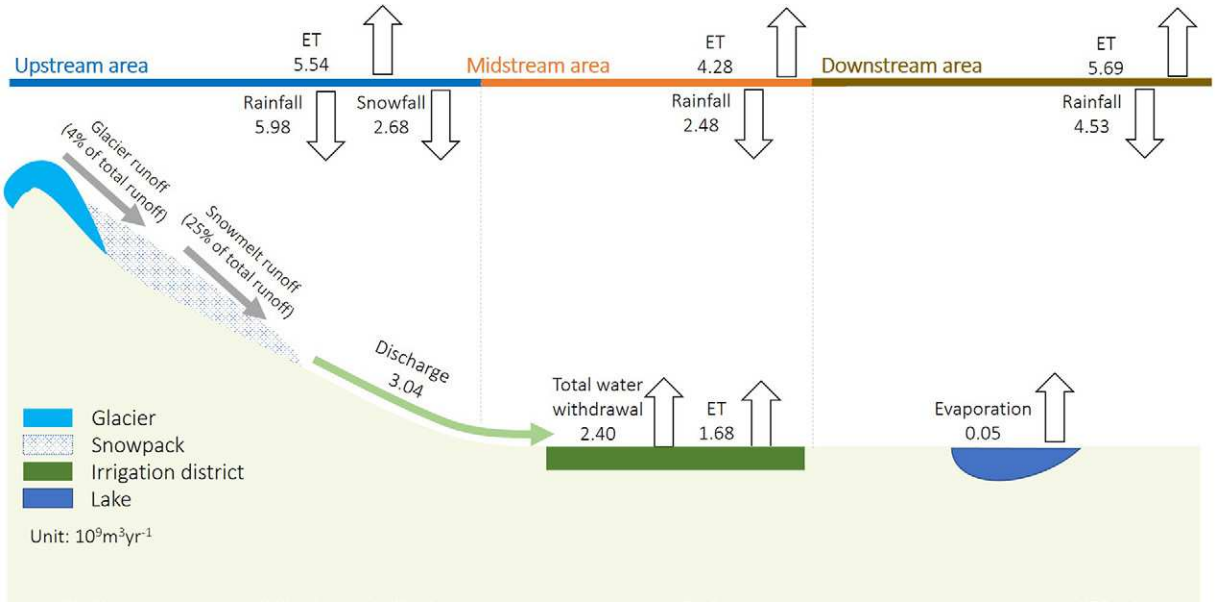

Fig. 13. The water balance in the Heihe River Basin (2001–2012). The result is calculated from the integrated modeling and the integrated observatory network. Precipitation, evapotranspiration (ET), discharges, and major landscapes are marked in the different regions (adapted from Li et al., 2018b).

resolution remote sensing products, and model–data integration in the HRB, have been accomplished; these accomplishments promote the integrated research of land surface processes in the HRB.

The observation experiences and findings in the HRB can be helpful to other endorheic basins in the "Silk Road Economic Belt" when building river-basin-scale observatories and conducting integrated experiments. Henceforth, the primary objective of the Heihe Integrated Observatory Network is to develop an intelligent monitoring system that incorporates ground-based observatory networks, unmanned aerial vehicles, and multisource satellites through Internet of Things technology. Meanwhile, biogeochemical process observation in the basin will be enhanced, and critical zone observations will be conducted, especially in the oasis–desert ecosystem. In the future, the observatory network will be extended to the entire Qilian Mountain region, which includes six inland rivers, of which the Heihe River is the largest. Integrating ground observations, remote sensing, and large-scale models is also among the main issues to be addressed in the Heihe Integrated Observatory Network, as this will enhance the predictive capabilities for basin-scale land surface processes and bolster the capacity to respond to water resource shortages and ecological environmental deterioration in an inland river basin due to rapid climate change and intensified human activities.

Acknowledgments

This work was supported by the Strategic Priority Research Program of the Chinese Academy of Sciences (Grant no. XDA20100101) and the National Natural Science Foundation of China (Grants no. 91425303, 41531174). We would like to thank all the scientists, engineers, and students who participated in HiWATER and WATER field campaigns.

References

André, J.C., J.P. Goutorbe, and A. Perrier. 1986. HAPEX-MOBLIHY: A hydrologic atmospheric experiment for the study of water budget and evaporation flux at the climatic scale. Bull. Am. Meteorol. Soc. 67:138–144. doi:10.1175/1520-0477(1986)067<0138:HAHAEF>2.0.CO;2

Ao, Y.H., S.H. Lv, S.Q. Chen, and Y. Zhang. 2005. Analyses of cold-wet tongue and boundary layer characteristic inside and outside of Jinta Oasis. (In Chinese.) Plateau Meteorol. 24(4):503–508.

Baldocchi, D., R. Valentini, S. Running, W. Oechel, and R. Dahlman. 1996. Strategies for measuring and modelling carbon dioxide and water vapour fluxes over terrestrial ecosystems. Global Change Biol. 2:159–168. doi:10.1111/j.1365-2486.1996.tb00069.x

Bogena, H., R. Bol, N. Borchard, N. Brüggemann, B. Diekkrüger, C. Drüe, et al. 2015. A terrestrial observatory approach to the integrated investigation of the effects of deforestation on water, energy, and matter fluxes. Sci. China Earth Sci. 58:61–75. doi:10.1007/s11430-014-4911-7

Cheng, G.D. 2009. Integrated management of the water–ecology–economy system in the Heihe River Basin. (In Chinese.) Science Press, Beijing.

Cheng, G.D., X. Li, W.Z. Zhao, Z.M. Xu, Q. Feng, S.C. Xiao, and H.L. Xiao. 2014a. Integrated study of the water–ecosystem–economy in the Heihe River Basin. Natl. Sci. Rev. 1:413–428. doi:10.1093/nsr/nwu017

Cheng, G.D., H.L. Xiao, B.J. Fu, D.N. Xiao, C.M. Zheng, S.Z. Kang et al. 2014b. Advances in synthetic research on the eco-hydrological process of the Heihe River Basin. (In Chinese, with English abstract.) Adv. Earth Sci. 29:431-437. doi:10.11867/j.issn.1001-8166.2014.04.0431

Cheng, G.D., and X. Li. 2015. Integrated research methods in watershed science. Sci. China Earth Sci. 58:1159–1168. doi:10.1007/s11430-015-5074-x

Fan, L., Q. Xiao, J.G. Wen, Q. Liu, Y. Tang, D.Q. You, et al. 2015. Evaluation of the airborne CASI/TASI Ts-VI space method for estimating near-surface soil moisture. Remote Sens. 7:3114–3137. doi:10.3390/rs70303114

Gao, B., D.W. Yang, Y. Qin, Y. Wang, H. Li, Y. Zhang, and T. Zhang. 2018. Change in frozen soils and its effect on regional hydrology, Upper Heihe Basin, northeastern Qinghai–Tibetan Plateau. Cryosphere 12:657–673. doi:10.5194/tc-12-657-2018

Ge, Y., Y.Z. Liang, J.H. Wang, Q.Y. Zhao, and S.M. Liu. 2015. Upscaling sensible heat fluxes with area-to-area regression kriging. IEEE Geosci. Remote Sens. Lett. 12:656–660. doi:10.1109/LGRS.2014.2355871

Goutorbe, J.P., T. Lebel, A. Tinga, P. Bessemoulin, J. Brouwer, A.J. Dolman, et al. 1994. HAPEX-Sahel: A large-scale study of land–atmosphere interactions in the semi-arid tropics. Ann. Geophys. 12:53–64. doi:10.1007/s00585-994-0053-0

Halldin, S., S.E. Gryning, L. Gottschalk, A. Jochum, L.C. Lundin, and A.A. Van de Griend. 1999. Energy, water and carbon exchange in a boreal forest landscape: NOPEX experiences. Agric. For. Meteorol. 98-99:5–29. doi:10.1016/S0168-1923(99)00148-3

Hu, G.C., and L. Jia. 2015. Monitoring of evapotranspiration in a semi-arid inland river basin by combining microwave and optical remote sensing observations. Remote Sens. 7:3056–3087. doi:10.3390/rs70303056

Hu, M.G., J.H. Wang, Y. Ge, M.X. Liu, S.M. Liu, Z.W. Xu, et al. 2015. Scaling flux tower observations of sensible heat flux using weighted area-to-area regression kriging. Atmosphere 6:1032–1044. doi:10.3390/atmos6081032

Hu, Y.Q., Y.X. Gao, J.M. Wang, G.L. Ji, Z.B. Shen, L.S. Cheng, et al. 1994. Some achievements in scientific research during HEIFE. (In Chinese, with English abstract.) Plateau Meteorol. 13:225–236

Huang, L., and X. Wen. 2014. Temporal variations of atmospheric water vapor dD and d^{18}O above an arid artificial oasis cropland in the Heihe River Basin. J. Geophys. Res. Atmos. 119:11456–11476. doi:10.1002/2014JD021891

Jensen, K.H., and T.H. Illangasekare. 2011. HOBE: A hydrological observatory. Vadose Zone J. 10:1–7. doi:10.2136/vzj2011.0006

Jin, R., X. Li, B.P. Yan, X.H. Li, W.M. Luo, M.G. Ma, et al. 2014. A nested eco-hydrological wireless sensor network for capturing surface heterogeneity in the midstream areas of the Heihe River Basin, China. IEEE Geosci. Remote Sens. Lett. 11:2015–2019. doi:10.1109/LGRS.2014.2319085

Jin, R., X. Li, and S.M. Liu. 2017. Understanding the heterogeneity of soil moisture and evapotranspiration using multiscale observations from satellites, airborne sensors and a ground-based observation matrix. IEEE Geosci. Remote Sens. Lett. 14:2132–2136. doi:10.1109/LGRS.2017.2754961

Kang, J., R. Jin, X. Li, and Y. Zhang. 2017. Block kriging with measurement errors: A case study of the spatial prediction of soil moisture in the middle reaches of Heihe River Basin. IEEE Geosci. Remote Sens. Lett. 14:87–91. doi:10.1109/LGRS.2016.2628767

Kuhlman, M.R., H. Loescher, R. Leonard, R. Farnsworth, T.E. Dawson, and E.F. Kelly. 2016. A new engagement model to complete and operate the national ecological observatory network. Bull. Ecol. Soc. Am. 97:283–287. doi:10.1002/bes2.1248

Li, X., X.W. Li, Z.Y. Li, M.G. Ma, J. Wang, Q. Xiao, et al. 2009. Watershed allied telemetry experimental research. J. Geophys. Res. Atmos. 114:D22103. doi:10.1029/2008JD011590

Li, X., G.D. Cheng, S.M. Liu, Q. Xiao, M.G. Ma, R. Jin, et al. 2013. Heihe Watershed Allied Telemetry Experimental Research (HiWATER): Scientific objectives and experimental design. Bull. Am. Meteorol. Soc. 94:1145–1160. doi:10.1175/BAMS-D-12-00154.1

Li, X., K. Yang, and Y.Z. Zhou. 2016. Progress in the study of oasis–desert interactions. Agric. For. Meteorol. 230–231:1–7. doi:10.1016/j.agrformet.2016.08.022

Li, X., S.M. Liu, Q. Xiao, M.G. Ma, R. Jin, T. Che, et al. 2017a. A multiscale dataset for understanding complex eco-hydrological processes in a heterogeneous oasis system. Sci. Data 4:170083. doi:10.1038/sdata.2017.83

Li, X., S.M. Liu, H.X. Li, Y.F. Ma, J.H. Wang, Y. Zhang, et al. 2018a. Intercomparison of six upscaling evapotranspiration methods: From site to the satellite pixel. J. Geophys. Res. Atmos. 123:6777–6803. doi:10.1029/2018JD028422

Li, X., G.D. Cheng, Y.C. Ge, H.Y. Li, F. Han, X.L. Hu, et al. 2018b. Hydrological cycle in the Heihe River Basin and its implication for water resource management in endorheic basins. J. Geophys. Res.

Atmos. 123:890–914. doi:10.1002/2017JD027889

Li, Y., C.L. Huang, J.L. Hou, J. Gu, G.F. Zhu, and X. Li. 2017b. Mapping daily evapotranspiration based on spatiotemporal fusion of ASTER and MODIS images over irrigated agricultural areas in the Heihe River Basin, Northwest China. Agric. For. Meteorol. 244-245:82–97. doi:10.1016/j.agrformet.2017.05.023

Liao, Y.R., W.J. Fan, and X.R. Xu. 2013. Algorithm of leaf area index product for HJ-CCD over Heihe River Basin. In: 2013 IEEE International Geoscience and Remote Sensing Symposium, Melbourne, VIC, Australia. 21–26 July 2013. IEEE, Piscataway, NJ. p. 169–172. doi:10.1109/IGARSS.2013.6721118

Liu, S.M., Z.W. Xu, W.Z. Wang, Z.Z. Jia, M.J. Zhu, and J.M. Wang. 2011. A comparison of eddy-covariance and large aperture scintillometer measurements with respect to the energy balance closure problem. Hydrol. Earth Syst. Sci. 15:1291–1306. doi:10.5194/hess-15-1291-2011

Liu, S.M., Z.W. Xu, Z.L. Zhu, Z.Z. Jia, and M.J. Zhu. 2013. Measurements of evapotranspiration from eddy-covariance systems and large aperture scintillometers in the Hai River Basin, China. J. Hydrol. 487:24–38. doi:10.1016/j.jhydrol.2013.02.025

Liu, S.M., Z.W. Xu, L.S. Song, Q.Y. Zhao, Y. Ge, T.R. Xu, et al. 2016. Upscaling evapotranspiration measurements from multi-site to the satellite pixel scale over heterogeneous land surfaces. Agric. For. Meteorol. 230–231:97–113. doi:10.1016/j.agrformet.2016.04.008

Liu, S.M., and Z.W. Xu. 2018. Micrometeorological methods to determine evapotranspiration. In: X. Li and H. Vereecken, editors, Observation and measurement of ecohydrological processes. Springer, Berlin. doi:10.1007/978-3-662-47871-4_7-2.

Lv, D.R., Z. Chen, J. Chen, G. Wang, J. Ji, H. Chen, and Z. Liu. 2002. Composite study on Inner Mongolia semiarid grassland soil–vegetation–atmosphere interaction (IMGRASS). (In Chinese.) Earth Sci. Front. 9(2):52–63

Lin, H., J.W. Hopmans, and D. Richter. 2011. Interdisciplinary sciences in a global network of critical zone observatories. Vadose Zone J. 10:781–785. doi:10.2136/vzj2011.0084

Ma, Y.F., S.M. Liu, L.S. Song, Z.W. Xu, T.R. Xu, and Z.L. Zhu. 2018. Estimating daily evapotranspiration and irrigation water efficiency at a Landsat-like scale using multi-source remote sensing data for a semi-arid irrigation area. Remote Sens. Environ. 216:715–734. doi:10.1016/j.rse.2018.07.019

Ma, Y.M., T.D. Yao, and J.M. Wang. 2006. Experimental study of energy and water cycle in Tibetan Plateau: The progress introduction on the study of GAME/Tibet and CAMP/Tibet. (In Chinese.) Plateau Meteorol. 25:344–351.

Mauder, M., S.P. Oncley, R. Vogt, T. Weidinger, L. Ribeiro, C. Bernhofer, et al. 2007. The energy balance experiment EBEX-2000: II. Intercomparison of eddy-covariance sensors and post-field data processing methods. Boundary-Layer Meteorol. 123:29–54. doi:10.1007/s10546-006-9139-4

Mu, X., S. Huang, H. Ren, G. Yan, W. Song, and G. Ruan. 2015. Validating GEOV1 fractional vegetation cover derived from coarse-resolution remote sensing images over croplands. IEEE J. Sel. Top. Appl. Earth Obs. Remote Sens. 8:439–446. doi:10.1109/JSTARS.2014.2342257

Nie, D., E.T. Kanemasu, L.J. Fritschen, H.L. Weaver, S.E.A. Smith, S.B. Verma, et al. 1992. An intercomparison of surface energy flux measurement systems used during FIFE 1987. J. Geophys. Res. 97(D17):18715–18724. doi:10.1029/91JD03044

Pan, X.D., X. Li, X.K. Shi, X.J. Han, L.H. Luo, and L.X. Wang. 2012. Dynamic downscaling of near-surface air temperature at the basin scale using WRF: A case study in the Heihe River Basin, China. Front. Earth Sci. 6:314–323. doi:10.1007/s11707-012-0306-2

Pan, X.D., X. Li, G.D. Cheng, H.Y. Li, and X.B. He. 2015. Development and evaluation of a river-basin-scale high spatio-temporal precipitation data set using the WRF model: A case study of the Heihe River Basin. Remote Sens. 7:9230–9252. doi:10.3390/rs70709230

Phinn, S., A. Specht, A. Lowe, M. Liddell, D. Lindenmayer, P. Grace, et al. 2011. Australia's TERN: Development a Terrestrial Ecosystem Research Network, building on past knowledge to generate new understanding. Paper presented at: 96th ESA Annual Meeting, Austin, TX. 7–12 Aug. 2011.

Qiao, C., R. Sun, Z.W. Xu, L. Zhang, L.Y. Liu, L.Y. Hao, and G. Jiang. 2015. A study of shelterbelt transpiration and cropland evapotranspiration in an irrigated area in the middle reaches of the Heihe River in northwestern China. IEEE Geosci. Remote Sens. Lett. 12:369–373. doi:10.1109/LGRS.2014.2342219

Qu, Y.H., Y.Q. Zhu, W.C. Han, J.D. Wang, and M.G. Ma. 2014. Crop leaf area index observations with a wireless sensor network and its potential for validating remote sensing products. IEEE J. Sel. Top. Appl. Earth Obs. Remote Sens. 7:431–444. doi:10.1109/JSTARS.2013.2289931

Ran, Y.H., X. Li, R. Sun, N. Kljun, L. Zhang, X.F. Wang, and G. Zhu. 2016. Spatial representativeness and uncertainty of eddy covariance carbon flux measurement for upscaling net ecosystem productivity to grid scale. Agric. For. Meteorol. 230–231:114–127. doi:10.1016/j.agrformet.2016.05.008

Sellers, P., F. Hall, H. Margolis, B. Kelly, D. Baldocchi, G. den Hartog, et al. 1995. The Boreal Ecosystem–Atmosphere Study (BOREAS): An overview and early results from the 1994 field year. Bull. Am. Meteorol. Soc. 76:1549–1577. doi:10.1175/1520-0477(1995)076<1549:TBESAO>2.0.CO;2

Sellers, P.J., F.G. Hall, G. Asrar, D.E. Strebel, and R.E. Murphy. 1988. The first ISLSCP field experiment (FIFE). Bull. Am. Meteorol. Soc. 69: 22–27. doi:10.1175/1520-0477(1988)069<0022:TFIFE>2.0.CO;2

Song, L.S., W.P. Kustas, S.M. Liu, P.D. Colaizzi, H. Nieto, Z.W. Xu, et al. 2016a. Applications of a thermal-based two-source energy balance model using Priestley–Taylor approach for surface temperature partitioning under advective conditions. J. Hydrol. 540:574–587. doi:10.1016/j.jhydrol.2016.06.034

Song, L.S., S.M. Liu, W.P. Kustas, J. Zhou, Z.W. Xu, T. Xia, and M.S. Li. 2016b. Application of remote sensing-based two-source energy balance model for mapping field surface fluxes with composite and component surface temperatures. Agric. For. Meteorol. 230–231:8–19. doi:10.1016/j.agrformet.2016.01.005

Song, L.S., S.M. Liu, W.P. Kustas, H. Nieto, L. Sun, Z.W. Xu, et al. 2018. Monitoring and validating spatially and temporally continuous daily evaporation and transpiration at river basin scale. Remote Sens. Environ. 219:72–88. doi:10.1016/j.rse.2018.10.002

Song, X.-D., D.J. Brus, F. Liu, D.-C. Li, Y.-G. Zhao, J.-L. Yang, and G.-L. Zhang. 2016. Mapping soil organic carbon content by geographically weighted regression: A case study in the Heihe River Basin, China. Geoderma 261:11–22. doi:10.1016/j.geoderma.2015.06.024

Tian, Y., Y. Zheng, C. Zheng, H. Xiao, W. Fan, S. Zou, et al. 2015. Exploring scale-dependent ecohydrological responses in a large endorheic river basin through integrated surface water–groundwater modeling. Water Resour. Res. 51:4065–4085. doi:10.1002/2015WR016881

Wang, J.M. 1999. Land surface process experiments and interaction study in China: From HEIFE to IMGRASS and GAME-Tibet/Tipex. (In Chinese, with English abstract.) Plateau Meteorol. 18:280–294.

Wang, P., X.-Y. Li, Y.M. Huang, S.M. Liu, Z.W. Xu, X.C. Wu, and Y.J. Ma. 2016. Numerical modeling the isotopic composition of evapotranspiration in an arid artificial oasis cropland ecosystem with high-frequency water vapor isotope measurement. Agric. For. Meteorol. 230–231:79–88. doi:10.1016/j.agrformet.2015.12.063

Wen, X.F., B. Yang, X. Sun, and X. Lee. 2016. Evapotranspiration partitioning through in-situ oxygen isotope measurements in an oasis cropland. Agric. For. Meteorol. 230-231:89–96. doi:10.1016/j.agrformet.2015.12.003

Xiong, Y., S.H. Zhao, F. Tian, and G.Y. Qiu. 2015. An evapotranspiration product for arid regions based on the three-temperature model and thermal remote sensing. J. Hydrol. 530:392–404. doi:10.1016/j.jhydrol.2015.09.050

Xu, Z.W., Y.F. Ma, S.M. Liu, W.J. Shi, and J.M. Wang. 2017a. Assessment of the energy balance closure under advective conditions and its impact using remote sensing data. J. Appl. Meteorol. Climatol. 56:127–140. doi:10.1175/JAMC-D-16-0096.1

Xu, F.N., W.Z. Wang, J.M. Wang, Z.W. Xu, Y. Qi, and Y.R. Wu. 2017b. Area-averaged evapotranspiration over a heterogeneous land surface: Aggregation of multi-point EC flux measurements with a high-resolution land-cover map and footprint analysis. Hydrol. Earth Syst. Sci. 21:4037–4051. doi:10.5194/hess-21-4037-2017

Xu, T.R., S.M. Bateni, S.A. Margulis, L.S. Song, S.M. Liu, and Z.W. Xu. 2016. Partitioning evapotranspiration into soil evaporation and canopy transpiration via a two-source variational data assimilation system. J. Hydrometeorol. 17:2353–2370. doi:10.1175/JHM-D-15-0178.1

Xu, T.R., Z.X. Guo, S.M. Liu, X.L. He, Y. Meng, Z.W. Xu, et al. 2018. Evaluating different machine learning methods for upscaling evapotranspiration

from flux towers to the regional scale. J. Geophys. Res. Atmos. 123:8674–8690. doi:10.1029/2018JD028447

Xu, Z.W., S.M. Liu, X. Li, S.J. Shi, J.M. Wang, Z.L. Zhu, et al. 2013. Intercomparison of surface energy flux measurement systems used during the HiWATER-MUSOEXE. J. Geophys. Res. Atmos. 118:13140–13157. doi:10.1002/2013JD020260

Yang, Y., D. Long, H. Guan, W. Liang, C. Simmons, and O. Batelaan. 2015a. Comparison of three dual-source remote sensing evapotranspiration models during the MUSOEXE-12 campaign: Revisit of model physics. Water Resour. Res. 51:3145–3165. doi:10.1002/2014WR015619

Yang, D.W., B. Gao, Y. Jiao, H.M. Lei, Y.L. Zhang, H.B. Yang, and Z.T. Cong. 2015b. A distributed scheme developed for eco-hydrological modeling in the Upper Heihe River. Sci. China Earth Sci. 58:36–45. doi:10.1007/s11430-014-5029-7

Yang, R.M., G.L. Zhang, F. Liu, Y.Y. Lu, F. Yang, F. Yang, et al. 2016. Comparison of boosted regression tree and random forest models for mapping topsoil organic carbon concentration in an alpine ecosystem. Ecol. Indic. 60:870–878. doi:10.1016/j.ecolind.2015.08.036

Yao, T.D., F.H. Chen, P. Cui, Y.M. Ma, B.Q. Xu, L.P. Zhu, et al. 2017a. From Tibetan Plateau to third pole and pan-third pole. (In Chinese.) Bull. Chin. Acad. Sci. 32:924–931. doi:10.16418/j.issn.1000-3045.2017.09.001

Yao, Y., S.L. Liang, J. Yu, J.Q. Chen, S.M. Liu, Y. Lin, et al. 2017b. A simple temperature domain two-source model for estimating agricultural field surface energy fluxes from Landsat images. J. Geophys. Res. Atmos. 122:5211–5236. doi:10.1002/2016JD026370

Zacharias, S., H. Bogena, L. Samaniego, M. Mauder, R. Fuß, T. Pütz, et al. 2011. A network of terrestrial environmental observatories in Germany. Vadose Zone J. 10:955–973. doi:10.2136/vzj2010.0139

Zhang, Y. 1998. Huaihe River Basin energy and water cycle experiment. (In Chinese.) Meteor. Sci. Technol. 4:33–38.

Zhang, Y., X.D. Huang, X.H. Hao, J. Wang, W. Wang, and T.G. Liang. 2014. Fractional snow-cover mapping using an improved endmember extraction algorithm. J. Appl. Remote Sens. 8(1):084691. doi:10.1117/1.JRS.8.084691

Zhong, B., A.X. Yang, A.X. Nie, Y.J. Yao, H. Zhang, S.L. Wu, and Q.H. Liu. 2015. Finer resolution land-cover mapping using multiple classifiers and multisource remotely sensed data in the Heihe River Basin. IEEE J. Sel. Top. Appl. Earth Obs. Remote Sens. 8:4973–4992. doi:10.1109/JSTARS.2015.2461453

Zhou, S., B.F. Yu, Y. Zhang, Y.F. Huang, and G.Q. Wang. 2018a. Water use efficiency and evapotranspiration partitioning for three typical ecosystems in the Heihe River Basin, northwestern China. Agric. For. Meteorol. 253:261–273. doi:10.1016/j.agrformet.2018.02.002

Zhou, Y.Z., D. Li, H.P. Liu, and X. Li. 2018b. Diurnal variations of the flux imbalance over homogeneous and heterogeneous landscapes. Boundary-Layer Meteorol. 168:417–442. doi:10.1007/s10546-018-0358-2

Zhu, Z.L., L. Tan, S.G. Gao, and Q.S. Jiao. 2015. Observation on soil moisture of irrigation cropland by cosmic-ray probe. IEEE Geosci. Remote Sens. Lett. 12:472–476. doi:10.1109/LGRS.2014.2346784